รายงานวิจัยฉบับสมบูรณ์

โครงการ การเคลือบไฮดรอกซีอะพาไทต์ – ปูนซีเมนต์ปอร์แลนด์ขาวบนโลหะ (เหล็กกล้าไร้สนิม) สำหรับวัสดุทดแทนกระดูก

โดย ผศ.ดร.ธีรวัฒน์ เหล่านภากุล

พฤษภาคม 2563

สัญญาเลขที่ MRG6180026

รายงานวิจัยฉบับสมบูรณ์

โครงการ การเคลือบไฮดรอกซีอะพาไทต์ – ปูนซีเมนต์ปอร์แลนด์ขาวบนโลหะ (เหล็กกล้าไร้สนิม) สำหรับวัสดุทดแทนกระดูก

ผู้วิจัย
ผศ.ดร.ธีรวัฒน์ เหล่านภากุล

สังกัด
มหาวิทยาลัยขอนแก่น

สนับสนุนโดยสำนักงานกองทุนสนับสนุนการวิจัย และมหาวิทยาลัยขอนแก่น
(ความเห็นในรายงานนี้เป็นของผู้วิจัย สกสว. ไม่จำเป็นต้องเห็นด้วยเสมอไป)

บทคัดย่อ

รหัสโครงการ: MRG6180026

ชื่อโครงการ: การเคลือบไฮดรอกซีอะพาไทต์ – ปูนซีเมนต์ปอร์แลนด์ขาวบนโลหะ (เหล็กกล้าไร้สนิม) สำหรับวัสดุทดแทนกระดูก

ชื่อนักวิจัย และสถาบัน: ผศ.ดร.ธีรวัฒน์ เหล่านภากุล มหาวิทยาลัยขอนแก่น

อีเมล์: teerla@kku.ac.th

ระยะเวลาโครงการ: 2 ปี

บทคัดย่อ: ไฮดรอกซีอะพาไทต์ (HAp) เป็นวัสดุที่เหมาะสำหรับทำไปใช้เป็นวัสดุซ่อมแซมหรือกระดูกเทียม ในขณะที่สมบัติทางกลของ HAp ไม่เหมาะกับงานที่ต้องรับภาระสูง ๆ เช่น การทดแทนการทำงานของกระดูก วัสดุผสม HAp/CK (Calcined kaolin) and HAp/WPC (White Portland cement) เป็นทางเลือกเพื่อให้เกิดการรวมกันของคุณสมบัติที่ดีที่สุดของวัสดุแต่ละชนิด ในการศึกษานี้ ได้ทำการศึกษาวิธีการเตรียมคอมโพสิต HAp/CK และ HAp/WPC การทดสอบสมบัติทางกลก่อนและหลังการทดสอบทางชีวภาพ และการทดสอบสมบัติทางกายภาพระหว่างการทดสอบทางชีวภาพของวัสดุผสมได้ถูกประเมินเพื่อนำมาใช้เป็นวัสดุทดแทนกระดูก นอกจากนี้ มีการนำโลหะที่เคลือบผิวด้วย HAp มาใช้อย่างกว้างขวางสำหรับการใช้งานด้านศัลยกรรมกระดูกและทันตกรรม เนื่องจากสามารถให้ความเข้ากันได้ทางชีวภาพที่ดีและคุณสมบัติเชิงกลที่ยอดเยี่ยม การเคลือบผิวด้วยวิธีการพลาสม่าสเปรย์เป็นหนึ่งในวิธีการที่ได้รับการยอมรับในการผลิตโลหะเคลือบผิวด้วย HAp สำหรับการใช้งานด้านการแพทย์ ข้อเสียของการเคลือบโดยวิธีนี้คือมีค่าใช้จ่ายค่อนข้างสูงและกระบวนการมีความซับซ้อนอุณหภูมิที่สูงมากของการพลาสม่าสเปรย์เป็นสาเหตุของการเปลี่ยนแปลงองค์กระกอบของสารเคลือบผิว ความไม่เสถียรระหว่างรอยต่อระหว่างโลหะและสารเคลือบผิว และความไม่แข็งแรงของผิวเคลือบเมื่อนำไปใช้ในภาวะความเค้นที่เปลี่ยนแปลงไปมาภายในร่างกาย ในการศึกษาครั้งนี้ได้มีการพัฒนากระบวนการเคลือบผิวโลหะแบบเย็นอย่างง่าย ๆ โดยการทดสอบการเคลือบ WPC ลงบนผิวของเหล็กกล้าไร้สนิมโดยผ่านหัวฉีดลมเย็นแรงดันสูงและทดสอบเพื่อให้ได้ชั้นเคลือบผิวที่มีความหนา 100-200 ไมโครเมตร การศึกษานี้มีวัตถุประสงค์หลักคือ 1) การพัฒนาเครื่องมือและกระบวนการเคลือบ HAp/WPC บนพื้นผิวของเหล็กกล้าไร้สนิม 2) การเตรียมและตรวจสอบคุณลักษณะของผง HAp/WPC 3) ทดสอบการเคลือบ HAp/WPC บนพื้นผิวของเหล็กกล้าไร้สนิม

คำหลัก : วัสดุทดแทนกระดูก การเคลือบวัสดุปลูกฝังในร่างกาย การทดสอบวัสดุชีวภาพ

Abstract

Project Code: MRG6180026

Project Title: Hydroxyapatite-White Portland cement Coating on Metal (Stainless Steel) for Bone Substitute Materials

Investigator: Asst. Prof. Teerawat Laonapakul

E-mail Address : teerla@kku.ac.th

Project Period : 2 years

Abstract: Hydroxyapatite (HAp) is an ideal material for artificial bone. While the mechanical properties of bulk HAp have been found to be unsuitable for load bearing applications such as orthopedics, HAp/CK (Calcined kaolin) and HAp/WPC (White Portland cement) composites are the alternative choices to achieve a combination of properties and also to incorporate the best characteristics of each of the component materials. In this study, the methods to prepare the HAp/CK and HAp/WPC composites were studied. The mechanical properties before and after *in vitro* test, physical properties and in vitro bioactivity tests of HAp/CK and HAp/WPC composites were investigated for used as bone substitute materials. In addition, HAp coated on metal implants have become widely used for orthopaedic and dental applications since it can provide a good biocompatibility with excellent mechanical properties. Plasma spraying is one of the commercially accepted methods to produce HAp coatings for biomedical applications. Unfortunately, disadvantages of the plasma spray process are relative high cost and complexity of process. The extremely high temperature of plasma spray is cause of decomposition of the coating, instability of coating-substrate interface and the unstable duration of coating under body fluids and varying local loading. In this study, a simple modified cold spray process in which the stainless-steel substrate was sprayed with WPC using high pressure cold air nozzle spray was designed to get the coatings thickness of 100-200 μm. The main focuses of this study are 1) the development of the novel spray tool and process of HAp-WPC coating on stainless-steel substrate 2) the preparation and characterization of HAp-WPC powder 3) the HAp-WPC coating on stainless steel substrate.

Keywords: Bone substitute materials, Coating implant, Biomaterial testing

Executive Summary

This research started from the synthesis of hydroxyapatite calcium phosphate bio-ceramic powder from the $CaCO_3$ and CaO (produced from golden apple snail shells) and dibasic calcium phosphate dihydrate ($CaHPO_4 \cdot 2H_2O$, DCPD) by using Solid-state reaction and mechanical activation. Hydroxyapatite (HAp) with a small quantity of β-TCP could be produced from the mixed $CaCO_3$+DCPD and mixed CaO+DCPD powders using dry mechanical activations combined with a solid-state reaction at a temperature of 1,100 °C. The methods to prepare the HAp/CK and HAp/WPC composites had been studied. *In vitro* bioactivity tests of HAp/CK and HAp/WPC composites with various mixing ratios were investigated for used as bone substitute materials. The mechanical property before and after *in vitro* test was conducted. The curing time and temperature significantly affected the compressive strength of HAp/CK samples, while there was no interaction between curing time and curing temperature. The highest compressive strength, 37.8 MPa (HAp/CK:25/75), was realized by curing the sample at 80 °C for 28 days. The optimal process was curing HAp/CK at 60 °C for 14 days to achieve a high compressive strength. The compressive strength of both WPC and HAp/WPC pastes increased with longer curing periods in water. The compressive strength of WPC and HAp/WPC (50:50) pastes was 51.88 and 25.67 MPa, respectively, after curing in water for 28 days. The addition of HAp into CK or WPC decreased the compressive strength of the sample. The strength of HAp/CK samples decreased with increasing the immersion periods in liquid solution after *in vitro* testing. On the other hand, the strength of HAp/WPC samples seem to increase with increasing the immersion periods in liquid solution. It was found that apatite formation took place on the surface of both samples, HAp/CK and HAp/WPC, after immersion in liquid solution for *in vitro* testing. The cold spray and processes of HAp/WPC coating on stainless steel substrate were developed. The primary study on the optimum parameters to achieve the coating thickness of 100-150 μm were investigated by using pure WPC. The results showed that the nozzle of 1.2 mm with the speed of the sample moving pass through the nozzle of 600 cm/min produced good surface condition and satisfying distribution of coating area on coated sample. In addition, a distance between the nozzle of 20 cm with twice coating times, was the optimum condition created 132 μm of coating thickness of the coated sample.

Objective

1. To study the synthesis of hydroxyapatite calcium phosphate bio-ceramic powder from the $CaCO_3$ and CaO (produced from golden apple snail shells)
2. To study the optimum conditions to prepare of the HAp/CK and HAp/WPC composites
3. To study and evaluate the use of the HAp/CK and/or HAp/WPC composite materials for medical application.
4. To develop the cold spray tool and process of HAp-WPC coating on stainless-steel substrate.
5. To study parameters that affect white Portland cement coating on 316L stainless steel using the cold spray technique in order to achieve 100-150 μm of coating thickness.

Research methodology

1. Raw material preparation and characterization

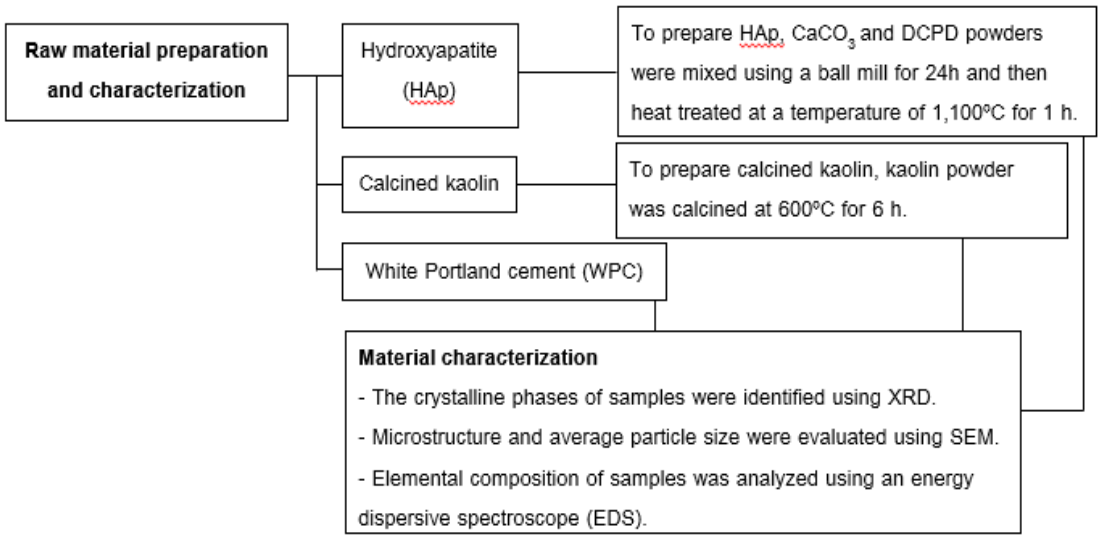

2. The preparation and characterization of HAp/CK and HAp/WPC composite materials

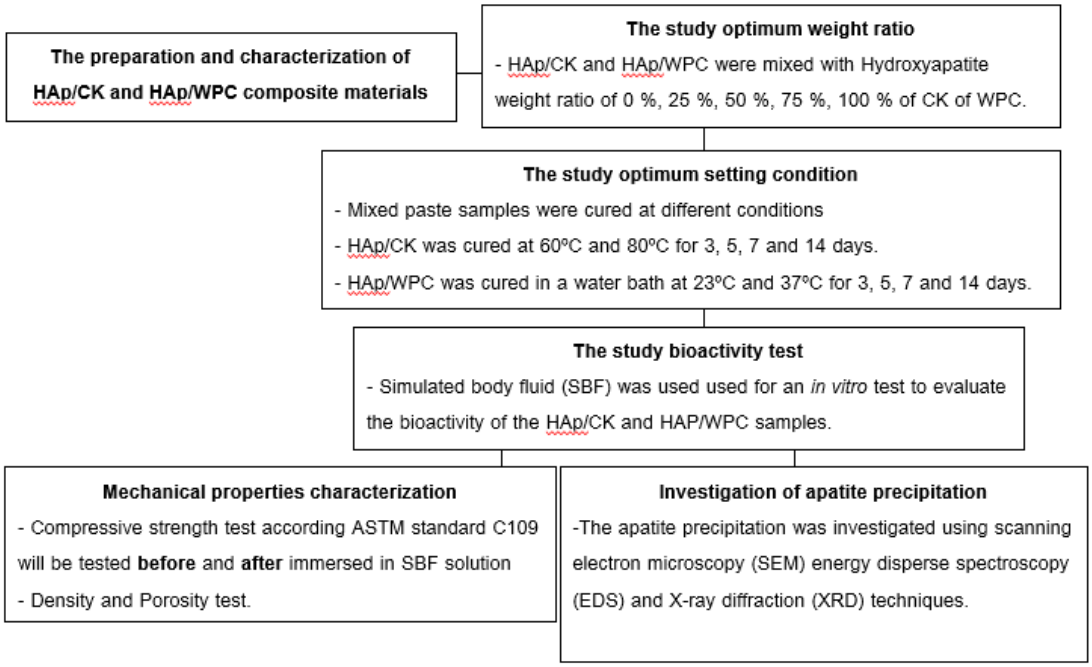

3. The development of the novel spray processes of HAp-WPC coating on stainless-steel substrate and characterization.
   - Design and construction the cold spray tools.
   - Design the preparation of stainless steel substrate surface.
   - Study HAp-WPC coating on stainless-steel substrate

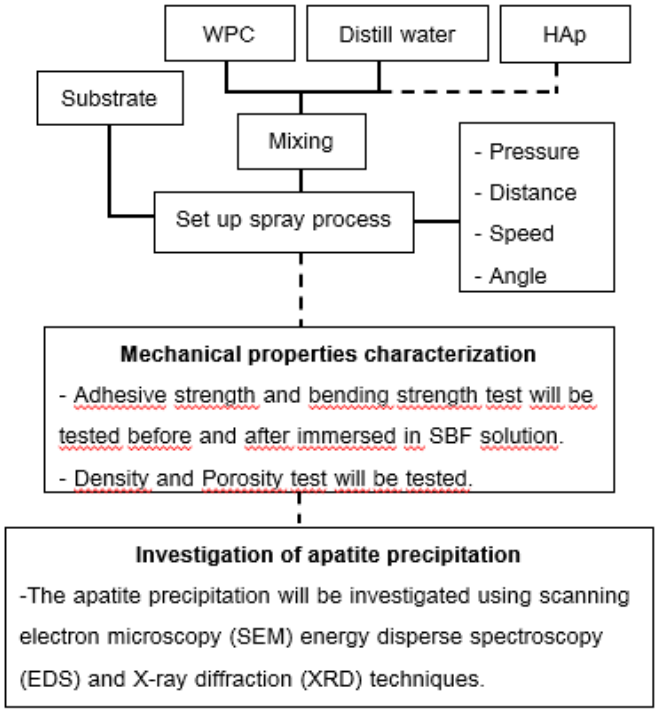

Research plan and future research

	Activities
Year 1: Month 1 – 8	**Raw material preparation and characterization** The preparation of $CaCO_3$ and CaO from golden apple snail shell The preparation of hydroxyapatite (HAp) from $CaCO_3$ and CaO **The preparation and characterization of HAp/CK and HAp/WPC composite materials** - The study optimum weight ratio - The study optimum setting and curing condition - Mechanical properties characterization **Writing up the manuscript** **Submission of the manuscript to the expected journal**
Year 1: Month 9 – 12 and Year 2: Month 1 – 12	**The preparation and characterization of HAp/CK and HAp/WPC composite materials (Cont.)** - The study bioactivity test - Investigation of apatite precipitation **The development of the novel spray processes coating on stainless-steel substrate and characterization** - Design and construction the cold spray tools. - Design the preparation of stainless steel substrate surface. - Study WPC coating on stainless-steel substrate **Writing up the manuscript** **Submission of the manuscript to the expected journal**
Continue Research	**The study of the HAp/WPC spray coating on stainless-steel substrate and characterization** - Mechanical properties characterization - Investigation of apatite precipitation **Writing up the manuscript** **Submission of the manuscript to the expected journal**

Results

The preparation of $CaCO_3$ and CaO from golden apple snail shell

Figure 1 shows the results of thermogravimetric analysis (TGA) of shell samples. The TGA curves for both types of shells were similar with three distinct stages of weight loss, as shown in Figs. 1. In the initial stage (I) at temperatures below 600 ºC, the weight of both shell samples decreased slightly by 2-3%. In the second stage (II) at temperatures between 600 and 800 ºC, the weights decreased rapidly until they had lost 44% of their weight. In the final stage (III) at temperatures above 800 ºC, the weight of shell samples remained almost constant. From the results, calcination temperatures of 600, 700, 800 and 900 ºC were selected to investigate the changes in elemental composition and transformation of the crystalline phases of shells. To study the influence of holding period on phase transformation, four different holding times, 1, 2, 3 and 4 hours, were used.

Golden apple snails (*Pomacca canaliculata*) are very serious invasive freshwater pests. They cause damage to agricultural products, especially rice and aquatic plants, leading to huge economic losses. It has been estimated that in Thailand, golden apple snails cause losses of at least 3,000 million US dollars annually. Nonetheless, they have been used as a protein source in animal feeds and human foods. The large consumption of blood cockle and golden apple snails results in a considerable amount of shell by-products that is now treated as waste. The three common mineral forms found in various shells are the aragonite, calcite and vaterite phases of calcium carbonate ($CaCO_3$). These shells are composed of 97-99% of $CaCO_3$ with some minor compounds, viz., MgO, Al_2O_3, Fe_2O_3, SiO_2, $Ca_3P_2O_8$, $CaSO_4$, proteins and mucopolysaccharides. Additionally, trace amounts of Sn, Mo, Mn, Cd, Ti, B, Pb, Au, Ag, Ni, Co, Bi, Cu, Sr, Rb and As are present.

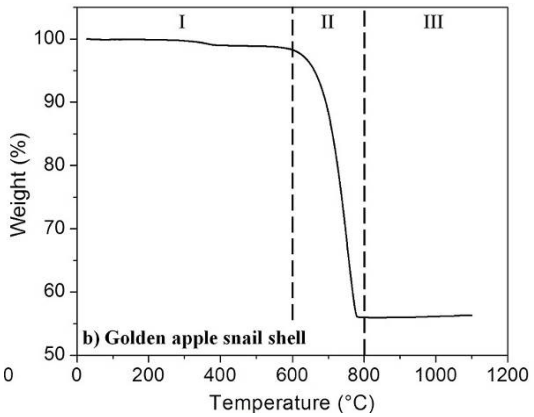

Fig. 1 TGA patterns of golden apple snail shell

Nowadays, research on the utilization of calcium compounds from seashells has attracted much interest. Numerous studies have been done with the aim of using alternative sources of $CaCO_3$ and CaO from various shells. However, insufficient information exists about the influence of calcination temperature and holding time on the phase transformations of $CaCO_3$ in shells that have a direct effect on the purity of the $CaCO_3$ and CaO phases. In the present study, transformations of the calcium phase of fresh water golden apple snail (GAS) shells were studied. The results showed that the pure $CaCO_3$ and CaO can be produced. Figures 2 (a-d) show XRD patterns of shells after calcination at temperatures of 600, 700, 800 and 900 ºC and 1-4 hour holding times.

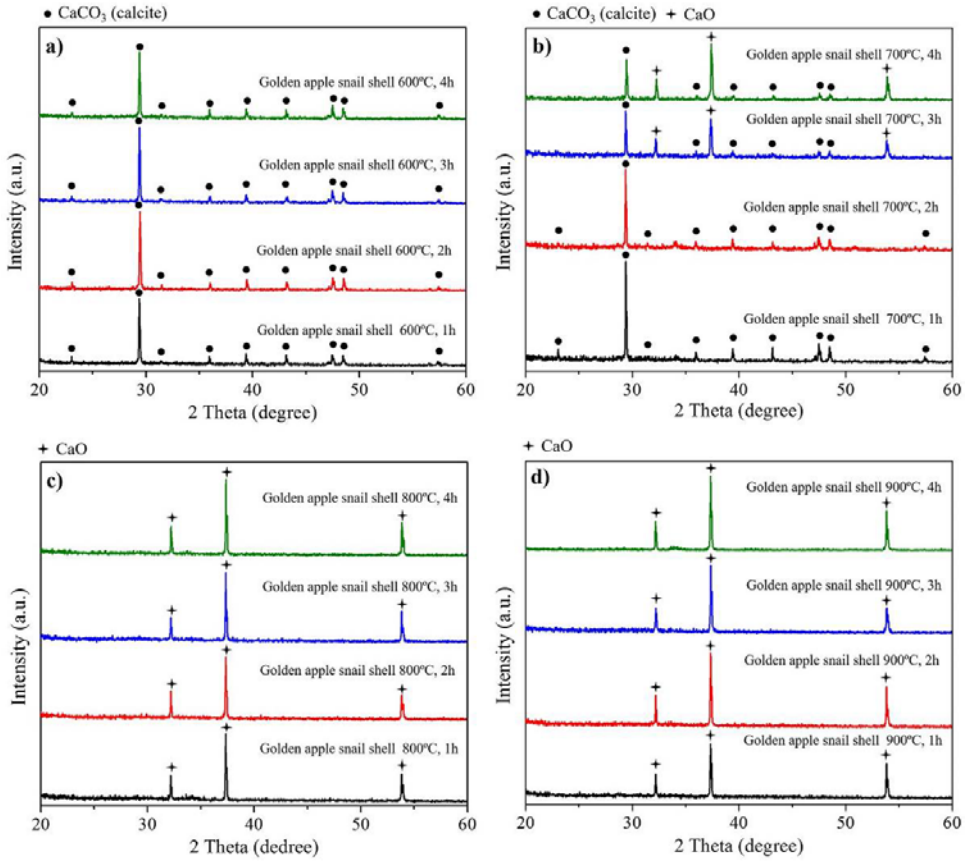

Fig. 2 XRD patterns of golden apple snail shell after calcination at (a) 600 ºC (b) 700 ºC (c) 800 ºC and (d) 900 ºC for various holding times

The XRD patterns of shells calcined at 600 ºC at all holding periods showed only the sharp characteristic peaks of a calcite phase, as shown in Figs. 2(a). For the samples calcined at 700 ºC, the single sharp characteristic peaks of a calcite phase was observed for GAS shells after a holding period of 1-2 hours, as depicted in Figs. 2(b). For the GAS shells calcined at 700 ºC for 3 and 4 hours, calcite co-existed with calcium oxide (CaO). This suggests that the phase transformation of $CaCO_3$ to CaO started at a

temperature between 700 and 800 ºC. The characteristic peaks associated with complete disappearance of the $CaCO_3$ phase after calcination at 800 ºC for all holding durations are shown in Figs. 2(c). When the calcination temperature was 900 ºC for all holding periods, only the characteristic peaks associated with CaO phase were observed, as shown in Figs. 2(d). This result indicated that amorphous $CaCO_3$ (aragonite) was completely transformed to crystalline $CaCO_3$ (calcite) and CaO at temperatures of 600 ºC and 800 ºC, respectively. The XRD results thus indicated that both calcination temperature and holding time were important for the phase transformation of $CaCO_3$ in shells.

Figures 3 shows scanning electron micrographs of shells that were calcined at 600, 700, 800 and 900 ºC for 1 hour. After calcination at 600 ºC, surface shells showed non-uniform irregular surfaces consisting of units up to 10-15 μm, as shown in Fig. 3(a). Increasing the temperature to 800 ºC and 900 ºC resulted in the formation of uniform micro-granules and fine grains (approximately 3-5 μm) of calcium compounds, as shown in Figs. 3(c, d). This change in surface morphology resulted from a transformation of the calcite phase of $CaCO_3$ to CaO, releasing CO_2 during high temperature calcination.

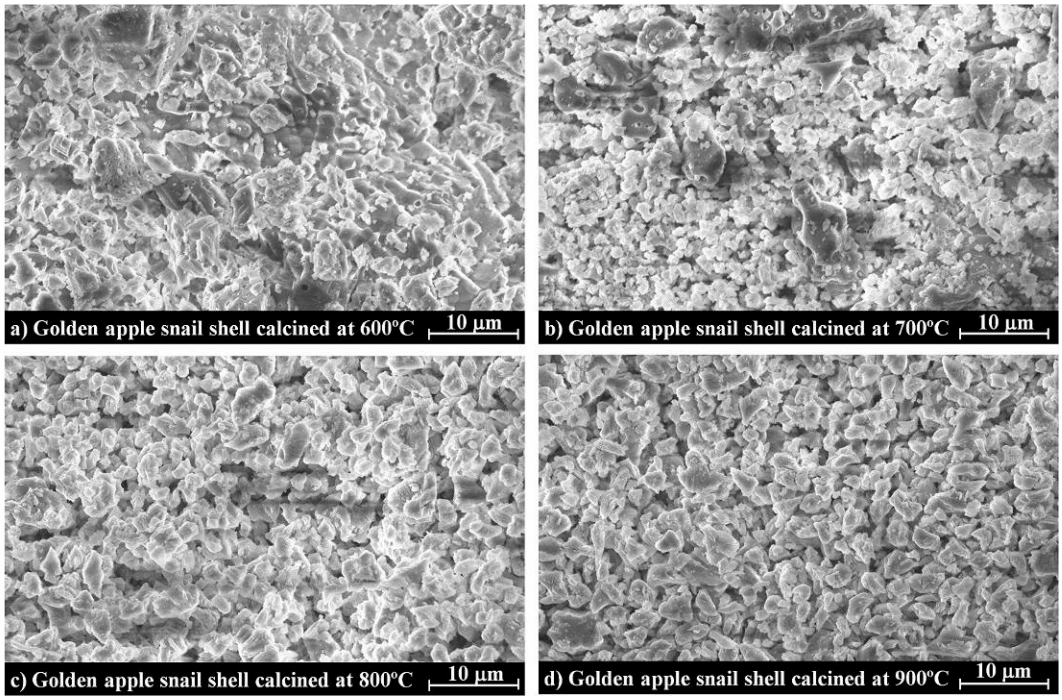

Fig. 3 SEM micrographs of surface morphology of golden apple snail shell after calcination at (a) 600 ºC (b) 700 ºC (c) 800 ºC and (d) 900 ºC

Many products, especially pharmaceutical materials and those for surgical implants (e.g., hydroxyapatite and beta tricalcium phosphate) require materials that are relatively free of heavy metal elements. Further investigation of the amount of As, Cd,

Hg, and Pb heavy metal elements was thus required. The presence of elements was quantitatively determined using inductively coupled plasma/mass spectroscopy (ICP-MS) on shell powders. The results, as shown in Table 1, indicate that the amounts of these elements in both raw and calcined shells (600 and 900 ºC) are very low. The GAS shells contained As, Cd, Hg or Pb concentrations exceeding the levels established by ASTM F1185-03 and ASTM F1108-04a required for ceramic hydroxyapatite and beta tricalcium phosphate for surgical implants derived from natural sources.

Table 1. Concentrations of heavy metal element in raw and calcined blood cockle and golden apple snail shells at 600 and 900 ºC for 1 hour

Elements	Golden apple snail shell (ppm)			ASTM F1185-03 and ASTM F1108-04a (ppm)
	Raw	600 ºC	900 ºC	
Arsenic (As)	0.049	0.137	0.145	5
Cadmium (Cd)	ND	ND	ND	3
Lead (Pb)	0.065	0.056	0.051	30
Mercury (Hg)	ND	ND	ND	5

* ND = Not Detected

The preparation of hydroxyapatite (HAp) from $CaCO_3$ and CaO

Calcium phosphate bioceramics, HAp and β-TCP in a powder form, have been widely studied and applied in biomedical applications, such as prosthetics and coating implants. In last two decades, biogenic structures and materials have been widely studied and used to produce calcium phosphate bioceramics (HAp and β-TCP) made via various synthesis techniques. Natural materials such as eggshells, seashells, animal bones and corals have been investigated as potential raw materials. The use of biogenic materials is an interesting approach to preparing calcium phosphate powders. They not only use biogenic resources, but economic and environmental benefits are obtained through waste recovery. Additionally, these studies have been motivated by constraints in generating synthetic materials. Previous study reported that the golden apple snail shell has significant potential for use as a raw calcium source in the synthesis of calcium phosphate powders.

In the present study, calcium carbonate and calcium oxide from golden apple snail shells and dicalcium phosphate dihydrate were used as the starting materials. This study aims at producing calcium phosphate bioceramics from golden apple snail shells

using a solid-state reaction or a mechanical process combined with a solid-state reaction. Calcium carbonate ($CaCO_3$) and calcium oxide (CaO) powders from calcined golden apple snail shells and dibasic calcium phosphate dihydrate ($CaHPO_4 \cdot 2H_2O$, DCPD) ($\geq$ 98%, Sigma-Aldrich, USA) were used as the starting materials. Appropriate amount of the mixture ratio of calcined golden apple snail shells (according to the calcium composition in calcined shells) to dibasic calcium phosphate dihydrate was carefully adjusted to obtain 100 g mixtures with the desired theoretical stoichiometric molar ratio (1.67) for HAp. The elemental compositions of $CaCO_3$ and CaO from calcined shells and raw shell were determined by using X-ray fluorescence. The results are presented in Table 2. The high proportions of calcium in shells calcined at 600 and 900 °C (96.2 and 98.3%, respectively) were presented. Other minor elements viz., Na, Sr, Cl, Si, Mg, S, Fe, Al, K, Mn and Ba were also presented.

Table 2 Elemental composition in raw and calcined golden apple snail shells at 600 and 900 °C for 1 hour

Element (%w)	CaO	Na_2O	SrO	Cl	SiO_2	MgO	SO_3	Fe_2O_3	Al_2O_3	K_2O	MnO	BaO
Raw	94.4	1.9	0.4	0.7	0.6	0.3	0.2	0.1	0.3	0.5	0.1	0.4
$CaCO_3$	96.2	1.4	0.2	0.6	0.5	0.2	0.1	0.1	0.2	0.1	0.1	0.3
CaO	98.3	0.8	0.3	0.2	0.1	0.1	0.1	-	0.1	-	0.1	0.1

Fig. 4 shows the XRD patterns of the starting powders ($CaCO_3$+DCPD and CaO+DCPD), manually mixed using a mortar and pestle (M-M) and mechanically mixed using a ball mill (B-M) without a liquid medium. As can be seen from Figs. 4 (a) and (b), the characteristic peaks of the starting powders were observed in M-M $CaCO_3$+DCPD and M-M CaO+DCPD mixed powders. The characteristic peaks of DCPD, CaO and calcium hydroxide ($Ca(OH)_2$) were observed in M-M CaO+DCPD mixed powders. The peak intensity of the starting powders ($CaCO_3$+DCPD) subjected to 24 hours of ball milling is presented in Fig. 4 (c). The decreasing and broadening of peak intensities of DCPD and $CaCO_3$ were observed compared with those of the starting powders mixed in a mortar and pestle (M-M $CaCO_3$+DCPD) (Fig. 4 (a)). This corresponds to the conversion of the starting materials to an amorphous form during ball mill. It is postulated that a slight reaction took place between starting materials after ball milling for 24 hours. The high intensity peaks of DCPD and CaO vanished from CaO+DCPD starting powders after being subjected to 24 hours of ball milling, as shown in Fig. 4 (d).

Weak and broad peaks corresponding to the HAp phase were clearly observed. This observation indicates that HAp had formed when the interfaces of the solid surfaces were in close contact during ball milling.

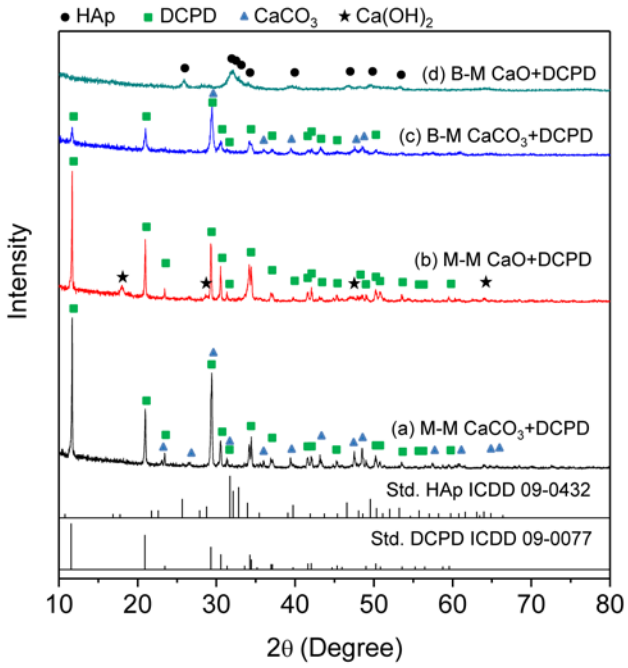

Fig. 3 The XRD patterns of the starting powders manually mixed using a mortar and pestle (a) M-M $CaCO_3$+DCPD (b) M-M CaO+DCPD and mechanically mixed during ball milling (c) B-M $CaCO_3$+DCPD (d) B-M CaO+DCPD without a liquid medium (ICDD No. 09-0432 for HAp and ICDD No. 09-0077 for DCPD)

The XRD patterns of powders ($CaCO_3$+DCPD and CaO+DCPD) manually mixed using a mortar and pestle (M-M) and ball milled (B-M) followed by calcination at 1,100 °C for 1 hour are shown in Fig. 4. The high intensity peaks characteristic of β-tricalcium phosphate (β-TCP, $Ca_3(PO_4)_2$) were primarily observed in the powders mixed with a mortar and pestle (M-M), as shown in Figs. 4 (a) and (b). In addition, the minor phase of HAp was also observed along with β-TCP phase. The high intensity peaks characteristic of HAp can be clearly seen on both patterns of the B-M $CaCO_3$+DCPD and B-M CaO+DCPD mixed powders after calcination at 1,100 °C for 1 hour. In addition to the peaks characteristic of HAp, those characteristics of β-TCP were also observed, as is shown in Figs. 4 (c) and (d). No peaks characteristic of the starting materials was found in any of the patterns.

As a result, it might be concluded that products derived from the mechanical activation and solid-state reactions of $CaCO_3$ or CaO + DCPD powders (Ca/P=1.67) were composed entirely of HAp crystals with a small quantity of β-TCP crystals. An

increase in the amount of Ca/P starting ratio may result in an actual stoichiometric Ca/P molar ratio.

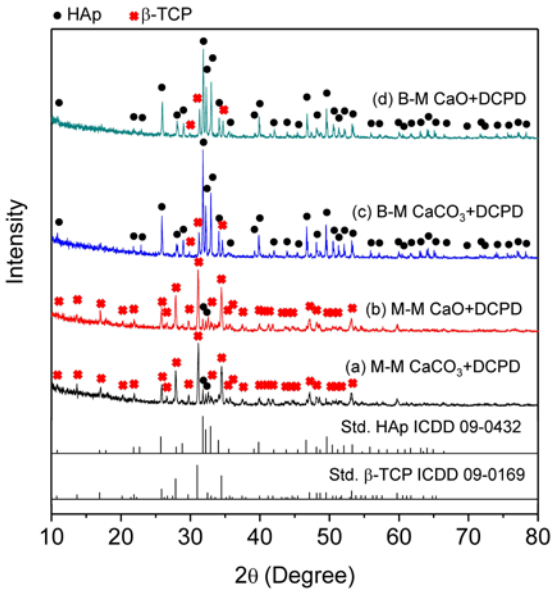

Fig. 4 The XRD patterns of the starting powders manually mixed using a mortar and pestle (a) M-M $CaCO_3$+DCPD (b) M-M CaO+DCPD and mechanically mixed during ball milling (c) B-M $CaCO_3$+DCPD (d) B-M CaO+DCPD without a liquid medium and then calcined at a temperature of 1,100 °C for 1 hour (ICDD No. 09-0432 for HAp and ICDD No. 09-0169 for β-TCP)

The study showed that β-TCP with a small amount of HAp was produced by manually mixed using a mortar and pestle (M-M) between $CaCO_3$ or CaO and DCPD and a solid-state reaction at 1,100 °C. The biphasic calcium phosphate (HAp/β-TCP) was produced by mechanically mixing during the ball milling (B-M) and the solid-state reaction at 1,100 °C.

The preparation and characterization of HAp/CK and HAp/WPC composite materials (Strength and bio activity test)

Hydroxyapatite (HAp) is an ideal material for artificial bone because it has excellent biocompatibility, bioactivity and osteoconductivity. Unfortunately, low strength and brittleness of HAp restrict its application only to bone repair. Calcined kaolin (CK) is one of several source materials used as a starting material to obtain a high strength in geopolymers. White Portland cement (WPC) is also a preferred choice to improve mechanical properties. While the mechanical properties of bulk HAp have been found to be unsuitable for load bearing applications such as orthopedics, HAp/CK and HAp/WPC composites are the alternative choices to achieve a combination of properties that is not

displayed by any single materials, and also to incorporate the best characteristics of each of the component materials. In this study, the methods to prepare the HAp/CK and HAp/WPC composites were studied.

The HAp/CK

The CK powder used in this study is mainly composed of 59.7% SiO_2 and 34.1% Al_2O_3. HAp and CK powders with HAP:CK weight ratio of 1:0(HAp100), 3:1(HAp75), 1:1(HAp50), 1:3(HAp25) and 0:1(HAp0) were prepared. Sodium hydroxide and sodium silicate with a weight ratio of 1:1 were prepared to use as a liquid binder. The ratio of 1:1 between mixed powder and liquid binder was used to prepare the HAp:CK paste samples. Paste samples were cast for compressive strength tests in 25x25x25 mm acyclic cube molds and for bioactivity test in 10 mm diameter and 2 mm thickness acyclic disc molds. Compressive strength tests were conducted on cube samples according to ASTM C109. Bioactivity tests were conducted on disc samples by immersion in simulated body fluid (SBF) in order to observe apatite precipitation on their surfaces.

Table 3 compares compressive strength of cured samples after storing at 23^{o}C for 7 days. The compressive strength of samples increased with the addition of an increased proportion of calcined kaolin (CK) into the HAp. The formation of cube and disc samples was not successful when the proportions of HAp were 75% and 100%. A higher compressive strength was observed for samples cured at 60^{o}C, when compared to those cured at 23^{o}C, for the same mixing conditions. For example, the strengths of HAp 25 cured at 23^{o}C and 60^{o}C were 32.19 MPa and 32.93 MPa, respectively. The addition of CK in HAp increases the amount of amorphous SiO_2 and Al_2O_3 in the system. The high amount of CK results in improvement of compressive strength due to the dissolution of silica and alumina species, subsequently promoting the polycondensation phenomena and the formation of polymeric binder, which results in the formation of C-S-H that acts as nucleating sites for geopolymer formation and accumulation. Therefore, the unformable HAp75 and HAp100 result from the less amount of silica and alumina species in sample.

Table 3 Compressive strength of the HAp-CK samples.

Curing temperature	Compressive strength (MPa)				
	HAp100	HAp75	HAp50	HAp25	HAp0
23°C	Not formation	Not formation	2.23	32.19	47.28
60°C			5.79	32.93	50.48

Surface morphology of disc samples for HAp0, HAp25 and HAp50 before and after immersion is SBF for 28 days were observed under an SEM, as show in Figure 5 (a-c). Figure 5 (a1, b1 and c1) show good flat surface morphology for all types of sample before immersion in SBF. The surface density of samples was found to decrease with increasing HAp weight ratio. Significant difference in surface morphology was not found between before and after immersion of HAp0 samples cured at 23^{o}C and 60^{o}C (Figure 5 (a1-a3)). The EDS spectrum of HAp0 cured at 60^{o}C after immersion in SBF for 28 days (Figure 5 (a4)) clearly shows the main spectrum peaks of aluminum (Al) and silicon (Si), which corresponds to the element composition of CK. The EDS spectra detected from samples cured at 23^{o}C and 60^{o}C after immersion in SBF show a similar pattern for each mixing ratio. It is seen from Figure 5 (b2, b3 and c2, c3) that the surface morphology of HAp25 and HAp50 samples changed its appearance from flat surfaces to small spherical particles after immersion in SBF for 28 days. The small spherical particles became dense with increasing weight ratio of HAp in CK. EDS spectra of HAp25 and HAp50 samples cured at 60^{o}C after immersion in SBF (Figure 5 (b4 and c4)) clearly show the spectrum peaks of calcium (Ca) and phosphorus (P) with Ca/P molar ratio of 1.225 and 1.616 respectively. The Ca/P molar ratio of these samples after immersion in SBF for 28 days was close to that of bone-like apatite (1.67). These results suggest that apatite precipitates in sample surfaces, as seen from Figure 5 (b2, b3 and c2, c3).

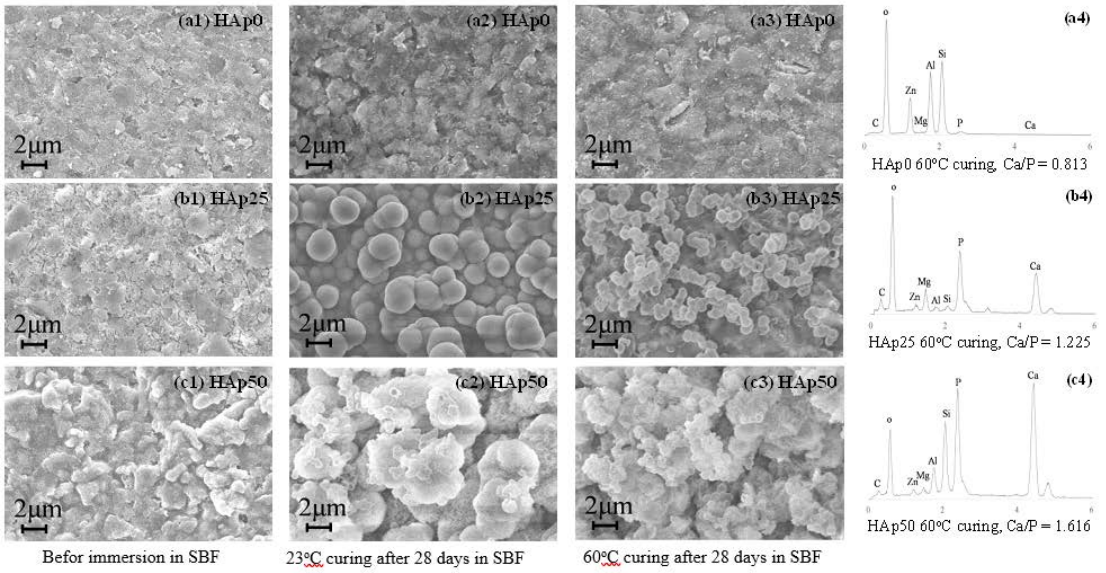

Fig. 5 SEM micrographs and EDS analysis of samples before and after immersion in SBF for 28 days (a) HAp0 (b) HAp25 and (c) HAp50

To confirm the result of apatite precipitation, the phase compositions on the surface of disc samples HAp0, HAp25, and HAp50 cured at 60°C before and after immersion in SBF for 28 days were investigated using XRD analysis. The results are shown in Figures 6 and 7. As seen from Figures 6 (a) and 7 (a), the XRD patterns of HAp0 show the characteristic peak of the silicon dioxide (SiO_2) phase, which corresponds to the CK. The characteristic peak of the HAp phase was not observed on both HAp0 samples before and after immersion in SBF. The XRD patterns for the HAp25 and HAp50 samples cured at 60°C before immersion in SBF are shown in Figure 6 (b and c). It is seen from the Figure that both samples composed of SiO_2 and HAp phases co-exist with the β-TCP phase. After immersion in SBF for 28 days, the high peak intensity of HAp was clearly observed on HAp50 sample and the peak intensity was lower on the HAp25 sample. However, the characteristic peak of the co-existing phase of β-TCP was not observed on HAp25 and HAp50 samples after immersion in SBF for 28 days, as seen from Figure 7 (b and c). The disappearance of β-TCP could result from the dissolution of β-TCP. An increased peak intensity of HAp phase after 28 days of immersion would suggest apatite precipitation in the sample surfaces.

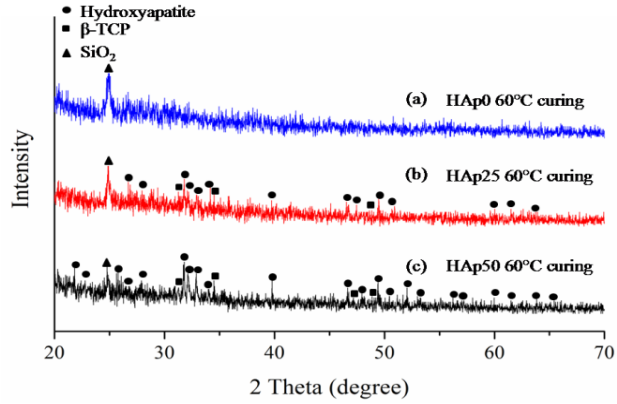

Fig. 6 XRD patterns of samples cured at 60°C before immersion in SBF (a) HAp0, (b) HAp25 and (c) HAp50

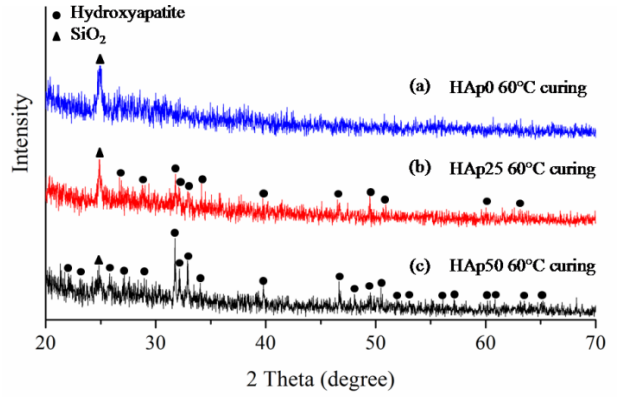

Fig. 7 XRD patterns of samples cured at 60°C after immersion in SBF for 28 days (a) HAp0, (b) HAp25 and (c) HAp50

The maximum compressive strength obtained from an HAp:CK mix at a ratio of 1:3 was 32.9 MPa when cured at 60ºC for 48 hours. This HAp:CK material exhibited good bioactivity after immersion in simulated body fluids for 28 days. However, varying curing time and temperature may have substantial effects on the ultimate properties of the final product. This study investigated the improved strength of HAp mixed with CK in terms of the curing regime used. The effect of curing time and temperature on the compressive strength of the HAp:CK final product was also investigated. Statistical analysis was done to determine the level of influence of each factor. SPSS was used assuming a normal distribution. Two-way ANOVA and Duncan's multiple range tests were used in the statistical analysis.

In this study, two factors were varied, curing temperature and time, to investigate their effect on the compressive strength of HAp/CK 25. Three curing temperatures, 40, 60 and 80ºC, and five curing times, 2, 7, 14, 21 and 28 days, were evaluated. Compressive strength tests were conducted on three cubed samples per each condition and the results were reported in the average values according to ASTM C109.

The statistical methodologies were employed to analyze the level of each factor using SPSS Version 19.0. This analysis began with checking the adequacy of the model by testing the normality of the parameter value distributions for all treatments using the Shapiro-Wilk's test (p-value>0.05), since there were less than 50 data points. Then, two-way analysis of variance (ANOVA) at a 95% confidence interval (α=0.05) was employed to test the differences between the mean values. Duncan's multiple range test was used to compare the means of the five levels of curing times (2, 7, 14, 21 and 28 days) and the three levels of curing temperature (40, 60 and 80ºC).

The average compressive strengths of samples cured at 40, 60 and 80ºC with various curing times are shown in Fig. 8. These three different curing temperatures were selected from observations of kaolin-based geopolymers, indicating that heat is beneficial for strength development and curing at temperatures below 100ºC, and that it has a significant contribution to the geopolymeric reaction in kaolin. The curing times of 2, 7, 14, 21 and 28 days were selected to allow sufficient time for the geopolymerization process. From Fig. 8, it can be seen that the strength of the samples increased with increasing curing time at all temperatures. The strength linearly increased with increasing curing time for the samples cured at 40ºC, whereas the strength of samples cured at 60 and 80ºC increased slightly over 7 days of curing. The highest strength, 37.8 MPa, was observed from samples cured at 80ºC for 28 days, while the compressive strength of cancellous bone is 2-45 MPa. From these results, it can be concluded that the appropriate curing conditions are a temperature of 80ºC for at least 7 days for strong development of HAp/CK 25. This range of strength is potential for cancellous bone graft substitute. Statistical analyses were used to elucidate the influence of curing time and temperature on the strength of HAp/CK 25 samples.

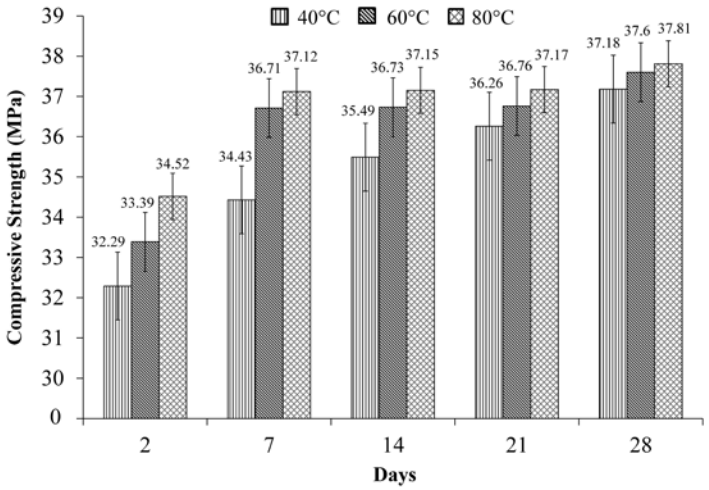

Fig. 8 Average compressive strengths of HAp/CK 25 samples after curing at 40, 60, and 80°C for various curing periods

A two-way analysis of variance (ANOVA) at a 95% confidence interval was employed to investigate the effects of curing temperature and time on the compressive strength of HAp/CK 25. The factors were considered separately and in aggregate. The results are shown in Table 4. The ANOVA results reveal that both curing time and curing temperature significantly affected (p-value<0.05) the compressive strength of HAp/CK 25, while the interaction between curing time and curing temperature had no significant effect (p-value>0.05) on the compressive strength of HAp/CK 25, as shown in Table 4. the Pearson correlation coefficient (Table 5) shows that the effects of curing time and temperature on compressive strength are related in a positive linear sense. The correlation value between curing time and compressive strength was 0.660 and between curing temperature and compressive strength was 0.359. This means the compressive strength of HAp/CK 25 increased with increasing curing time. Also, at a higher curing temperature, the compressive strength was greater than at a lower curing temperature. Moreover, it was found that the correlation between curing time and compressive strength was much stronger than that between curing temperature and compressive strength (0.660>0.359) as is shown in Table 5.

Table 4. Two-way ANOVA test of the effects of curing temperature and time on the compressive strength of HAp/CK 25

Tests Factor Interaction Effects

Dependent Variable: Strength

Source	Type III Sum of Squares	df	Mean Square	F	Sig.
Corrected Model	114.905[a]	14	8.207	6.335	0.000
Intercept	58459.475	1	58459.475	45124.159	0.000
Day	88.604	4	22.151	17.098	0.000
Temp	20.622	2	10.311	7.959	0.002
Day * Temp	5.680	8	0.710	0.548	0.811
Error	38.866	30	1.296		
Total	58613.246	45			
Corrected Total	153.770	44			

a. R^2 = .747 (Adjusted R^2 = .629)

Table 5. Pearson correlation of curing time and curing temperature with the compressive strength of HAp/CK 25

Correlations

		Day	Temp	Strength
Day	Pearson Correlation	1	0.000	0.660
	Sig. (2-tailed)		1.000	0.000
	N	45	45	45
Temp	Pearson Correlation	0.000	1	0.359
	Sig. (2-tailed)	1.000		0.016
	N	45	45	45
Strength	Pearson Correlation	0.660	0.359	1
	Sig. (2-tailed)	0.000	0.016	
	N	45	45	45

Duncan's multiple range test was then used to compare the range of a subset of the compressive strengths of HAp/CK 25 based on curing time and another range of a subset of the compressive strengths of HAp/CK 25 based on curing temperature. The results are shown in Table 6.

Table 6. Duncan's multiple range test of curing temperature and curing time on the compressive strength of HAp/CK 25

Cured time	N	Subset 1	Subset 2	Subset 3
2.00	9	33.4027		
7.00	9		36.0889	
14.00	9		36.4551	36.4551
21.00	9		36.7342	36.7342
28.00	9			37.5342
Sig.		1.000	0.266	0.066

Cured temp.	N	Subset 1	Subset 2
40.00	15	35.1339	
60.00	15		36.2379
80.00	15		36.7573
Sig.		1.000	0.221

N – Sample size; Sig. – significance

The compressive strength of HAp/CK 25 increased significantly with increased curing time. However, there were no significant differences in the compressive strengths of HAp/CK 25 after 7, 14 and 21 days of curing at a 95% confidence interval. The highest compressive strength, 36.7 MPa, was observed after 21 days. Moreover, after

14, 21 and 28 days of curing, there were no significant differences in the compressive strengths of HAp/CK 25 at a 95% confidence interval. The highest compressive strength, 37.5 MPa, was after 28 days.

The compressive strength of HAp/CK 25 increased significantly with increased curing temperature. There were significant differences in compressive strength of HAp/CK 25 with curing at 40ºC among all pairs of curing temperatures at a 95% confidence interval. However, there were no significant differences in compressive strength of HAp/CK 25 with curing at 60ºC and 80ºC with a 95% confidence interval. The highest compressive strength, 36.8 MPa, was observed after curing at 80ºC. From these results, it can be concluded that curing at 60ºC for 14 days represents the optimal curing conditions to achieve the maximal compressive strength of HAp/CK 25.

The HAp/WPC

The starting materials used in this research were commercial white Portland cement (WPC) and hydroxyapatite (HAp) powders. The WPC powder used in this study had chemical composition consisting of 14.67% SiO_2, 1.93% Al_2O_3, 78.77% CaO, 0.328% Fe_2O_3, 0.31% MgO, 0.04% Na_2O, 3.22% SO_3, and 0.13% TiO. In this research, pure WPC (denoted as WPC) powder and mixed of WPC and HAp (denoted as HAp/WPC) powders with a weight ratio of 1:1 were prepared. The mixed powders were blended with distilled water in a solid to liquid ratio of 2:1 by using mechanical mixing machine to prepare pastes of the samples. These pastes were cast into cubic molds (25 mm^3) for compressive strength testing, and disk-shaped molds (diameter 10 mm, 2 mm thick) for bioactivity testing. Then, they were vibrated for 10 seconds to remove entrapped air. All samples were wrapped in plastic sheets to control moisture loss and were stored to set in controlled room at a temperature of 23 °C for 24 hours before testing.

The samples cured in pure water for 28 days and were immersed in SBF and in pure water for 3, 7, 14, and 28 days. Compressive strength tests were conducted according to ASTM C109. After setting under controlled conditions, disk-shaped paste samples were removed from their molds and cured in pure water at 23 °C for 28 days. These samples were then immersed in a SBF solution at 37 °C for 7 days. The SBF solution had an ion profile and concentration close to that of human blood plasma. Bioactivity tests were conducted by observing the formation of bone-like apatite on the sample surfaces.

The results of compressive strength development of WPC and HAp/WPC pastes during water curing and during immersion in a SBF solution are shown in Fig.1. As the length of time for water curing was extended, the compressive strength of both types of samples increased (Fig. 9 (a)), as cement hydration was gradually accomplished. When WPC reacted with water, it underwent a hydration process forming ettringite, calcium silicate hydrate and calcium hydroxide, all of which contributed to the strength development seen in the WPC samples. After curing in water for 28 days, the compressive strength achieved by the WPC and HAp/WPC samples was 51.88 and 25.67 MPa, respectively. The addition of HAp to WPC affected the hydration of WPC resulting in a deceased compressive strength. Both of these sample types have potential for use in cancellous bone applications as their compressive strengths are within the range of that of cancellous bone (2-45 MPa).

After curing in water for 28 days, both samples types were immersed in SBF for 3, 7, 14 and 28 days and then subjected to compression testing. The results are shown in Fig. 1 (b). It can be seen from this figure that the compressive strength of WPC and HAp/WPC samples gradually increased to 59.02 and 28.06 MPa, respectively, after four weeks of immersion in SBF solution. The increased strength of WPC after immersion in SBF solution may have been due to continued hydration of the samples. The increasing compressive strength of the WPC samples was greater than that of HAp/WPC samples based on the purity of WPC. However, the increased strength of these specimens after immersion in SBF solution is a good indicator that they can be used as a bone substitute material for implantation in a physiological environment.

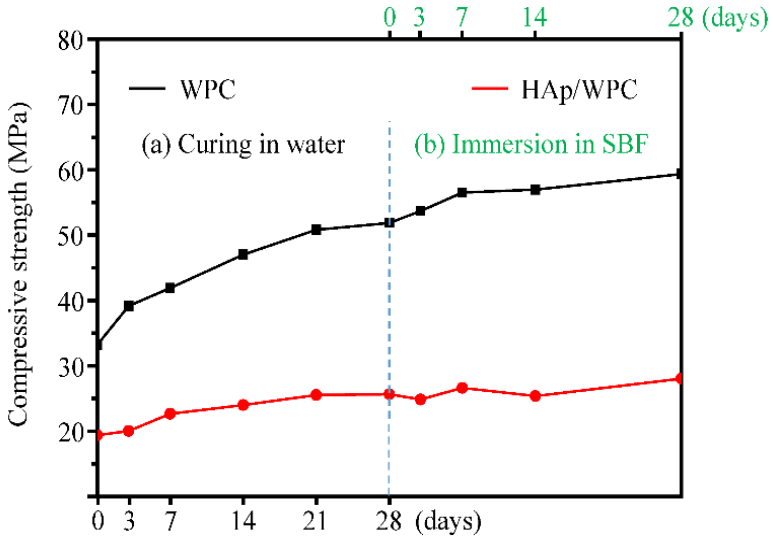

Fig.9 Compressive strength of the WPC and HAp/WPC samples

Fig. 10 shows the XRD patterns of the as-cured WPC and HAp/WPC samples and those of these samples after immersion in SBF solution for 7 days. The XRD patterns of the as-cured WPC and HAp/WPC samples are shown in Fig. 10 (a). The major crystalline phases detected in both samples were calcite, portlandite and ettringite, which are the crystalline phases found in hydrated cement. Excluding the crystalline phases of hydrated cement, the characteristic peaks of the HAp phase were detected on the HAp/WPC sample due to the addition of HAp during the sample preparation. The XRD patterns of the WPC and HAp/WPC samples after immersion in SBF solution for 7 days are shown in Fig. 10 (b). Changes in the phase composition of both samples were observed. The peak intensity of the portlandite phase disappeared after 7 days of immersion, whereas those of calcite and ettringite phases decreased after immersion in SBF solution for 7 days. From the results, it can be concluded that these three phases dissolved in the SBF solution.

An increasingly broad peak intensity of a HAp phase was observed at about 2θ = 25.8° and 31-33° on WPC samples after 7 days of immersion, as shown from Fig. 10 (b). The peak intensity of the HAp phase of HAp/WPC changed its appearance from a sharp to broad peak intensity after 7 days of immersion. These results implied that the amorphous phase of bone-like apatite was precipitated on the surfaces of both samples. The composition of the dissolved of phase of WPC increased the degree of supersaturation in the SBF solution by increasing the ionic activity of apatite and accelerated bone-like apatite nucleation on the surfaces.

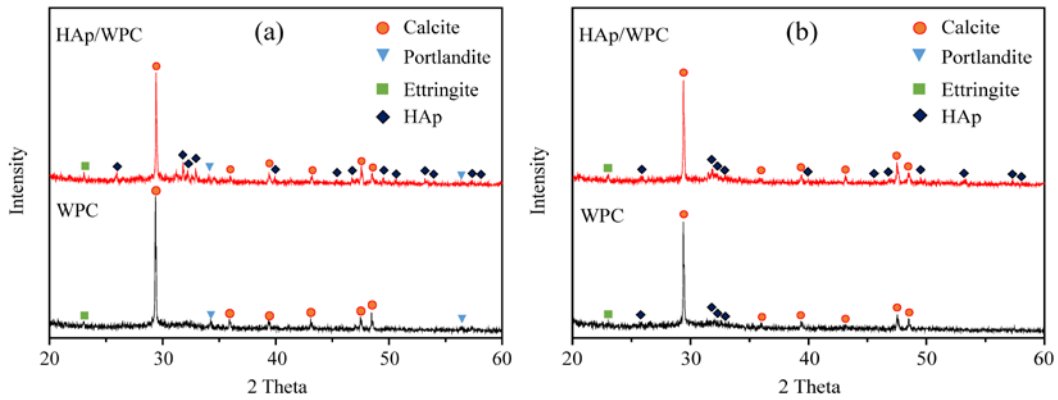

Fig. 10 XRD patterns of samples (a) as-cured and (b) after immersion in SBF for 7 days for WPC and HAp/WPC

Fig. 11 shows the morphological changes observed on the as-cured WPC and HAp/WPC sample surfaces. Fig. 11 (a) displays a homogeneous structure showing the compacted surface of the WPC sample before immersion. Irregularly shaped WPC particles were observed on its surface. For the HAp/WPC before immersion, irregularly

shaped WPC particles were mixed with round HAp particles as shown in Fig. 11 (b). EDS analysis of the WPC and HAp/WPC surfaces before immersion in the SBF solution are shown in Fig. 11 (c) and (d), respectively. The presence of calcium (Ca), silicon (Si), magnesium (Mg) and aluminum (Al) was observed. An aurum (Au) peak intensity was detected due to the Au coating applied prior to SEM observations. Phosphorus (P) was detected on the HAp/WPC surfaces due to the HAp present in this type of sample. A low intensity peak of P was detected and was difficult to observe due to the small amounts of phosphate compounds. The peak intensity of P was nearly equal to that of Au.

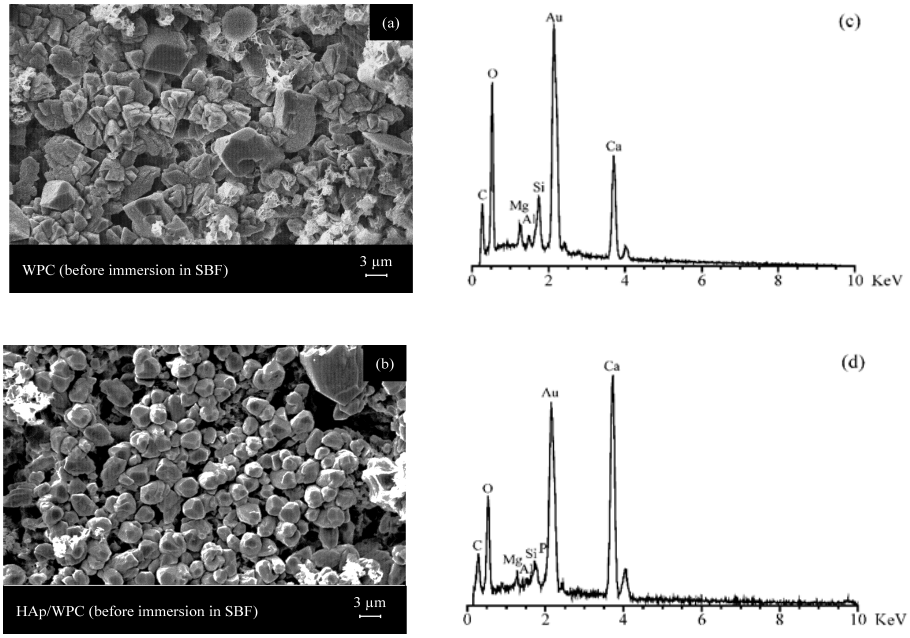

Fig. 11 SEM/EDS micrograph showing morphological changes on sample surfaces of the as-cured WPC and HAp/WPC samples: (a) SEM micrograph of the WPC sample, (b) SEM micrograph of the HAp/WPC sample (c) EDS analysis of the WPC sample, and, (d) EDS analysis of the HAp/WPC sample

Fig. 12 shows the morphological changes of WPC and HAp/WPC surfaces after immersion in SBF solution for 7 days. The surface texture of the WPC and HAp/WPC samples changed so that it had highly porous surfaces with tiny spherical particles, as presented in Fig. 12 (a) and (b). The spherical particles on the HAp/WPC surfaces were larger than those on the WPC surfaces. Fig. 12 (c) and (d) show the EDS spectra of the WPC and HAp/WPC surfaces after immersion in SBF solution for 7 days. A high intensity peak of the P spectrum was clearly observed in addition the Ca, Si and Mg spectra. A stronger intensity peak of P spectrum was observed in the HAp mixed sample. The SEM observations, EDS and XRD analysis confirmed precipitation of a

bone-like apatite on the WPC and HAp/WPC sample surfaces during immersion in the SBF solution.

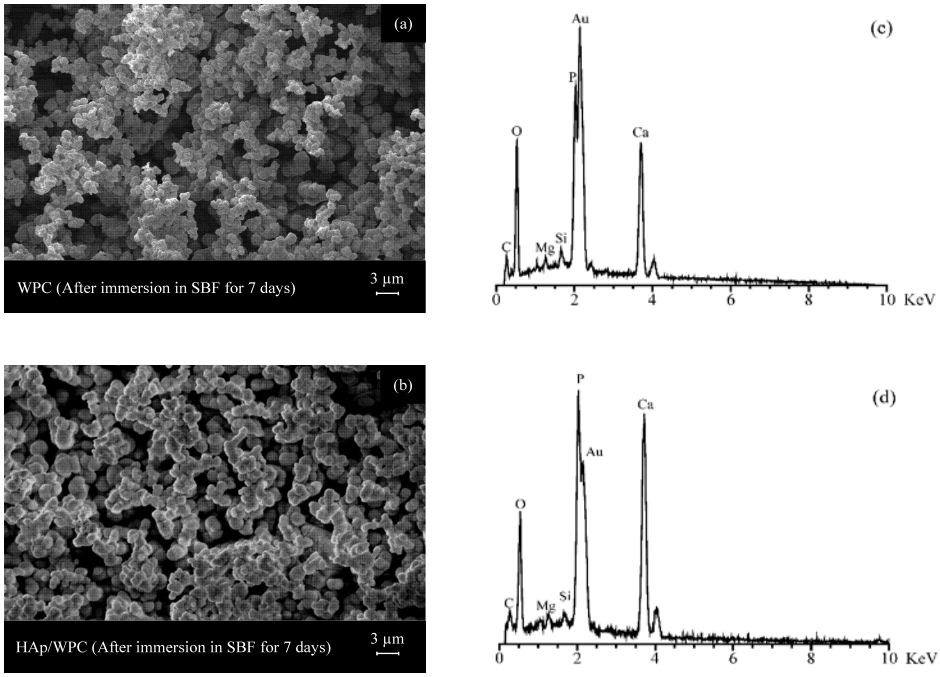

Fig. 12 SEM/EDS of surface morphological changes of WPC and HAp/WPC after immersion in SBF solution for 7 days: (a) SEM micrograph of a WPC sample, (b) SEM micrograph of a HAp/WPC sample, (c) EDS analysis of a WPC sample, and, (d) EDS analysis of a HAp/WPC sample

The development of the novel spray processes coating on stainless-steel substrate and characterization

This research aims to study parameters that affect white Portland cement coating on 316L stainless steel using the cold spray technique in order to achieve 100-150 µm of coating thickness. The evaluation parameters, which were studied are: 1) speed of the sample moving pass through the spray nozzle 2) size of the spray nozzle 3) distance between the coating nozzle and sample surface 4) coating repetition. After the cold spray process, the thickness of the specimen is analyzed using an optical microscope.

The stainless steel grade 316L is material that is widely used in surgery due to its good corrosion resistant and the ability to be compatible with human tissue. However, the stainless steels may corrode inside the body under certain circumstances in a highly stressed and oxygen depleted region, such as the contacts under the screws of the bone fracture plate. Therefore, this materials is suitable to use only in temporary implant devices. To improve their bioactivity, stainless steel usually coated with

hydroxyapatite (Hap), which has been widely used in medical applications due to their favorable biocompatibility and osteoconductivity. Therefore, a bioactive HAp coating on stainless steel surface would be one of the most promising implant materials of a good combination of coating biocompatibility and substrate strength. The plasma spraying is now widely accepted method for HAp coating because it gives tight adhesion between HAp and metal substrate with a coating thickness about 100 to 150 μm. Unfortunately, disadvantages of the plasma spray process are relative high cost and complexity of process. Moreover, The extremely high temperature of plasma spray is cause of decomposition of the coating, instability of coating-substrate interface, thermal expansion mismatch, residual stress in coating layer and unstable duration of coating under body fluids and varying local loading. Therefore, novel cold spray coating is an interesting technology need to be studied to obtain surface coating. This technique may offer several technological advantages over thermal spray, for examples, tensile residual stress, thermal decomposition and instability of coating-substrate interface may be avoided. However, the formation of HAp coating on the metal substrate at low temperature is a limitation. In order to solve this restriction, White Portland cement (WPC) is the prefer choice to study since its setting behavior and strength development are essentially the same as that expected in gray cement. WPC based materials have been proved non-toxic and feasibility of obtaining biocompatibility and bioactivity. It has potential to promote bone healing and bone tissue engineering application. Moreover, WPC has also been proved the feasibility of obtaining bioactivity for bone tissue engineering application. In addition, white color of WPC seems to be suitable source material for bone substitute materials.

The principal objective of this study to develop the novel spray tool and process of WPC coating on stainless-steel substrate and to evaluate the optimum parameters to achieve the coating thickness at 100 - 150 μm. The evaluation parameters, which were studied are: 1) spray nozzle size 2) speed of the sample moving pass through the spray nozzle 3) distances between coating nozzle and sample surface 4) coating repetition.

The SUS 316L was cut to a shape of rectangular with a size of 10x3x20 mm. They were then sand-blasted in order to get average roughness (Ra) of 3-6 μm. The WPC powder was sifted through a 100-mesh screen and then mixed with distilled water at a ratio of 1: 0.5 by weight before spraying. Fig. 13 shows schematic design of cold spray coating equipment, which is compose of: 1) air compressor 2) spray gun with three different sizes of nozzle 3) coating table, which can adjust the speed of sample moving and coating distance and 4) coating repetition. In this study, these parameters

were selected to study the suitable coating condition to achieve optimum coating thickness of 100-150 μm, as follow: 1) sizes of the spray nozzle of 1.2, 1.7 and 2.0 mm. 2) speeds of sample moving pass through the spray nozzle of 600, 1,200 and 1,800 cm/min 3) distances between the spray nozzle and sample of 15, 20, 25 and 30 cm. and 4) coating repetition of 1, 2 and 3 times. For each condition, the air pressure from compressor was fix at appropriate pressure of 0.3 MPa.

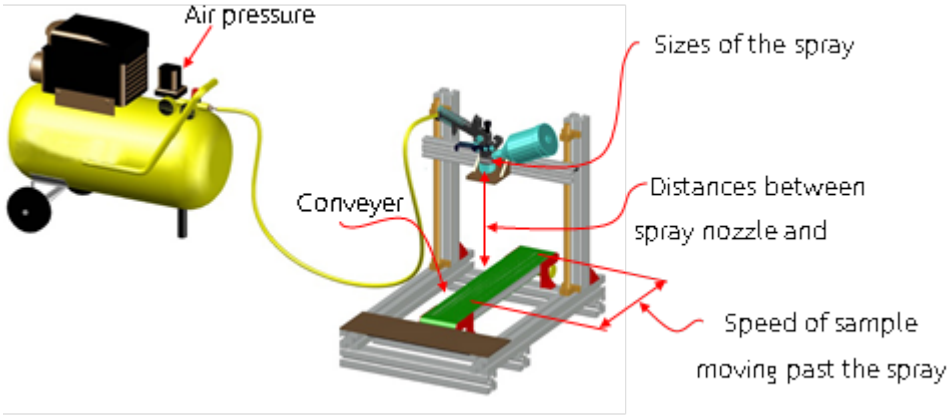

Fig. 13 Schematic design of cold spray coating equipment

After spraying, the coated samples were leaved at ambient temperature for 1 hour and cured in water for 24 hours to allow the coating layer setting. The coated samples were then mounted into resin and allowed them to solidify at room temperature for 24 hours. The mounted samples were polished with sandpaper and diamond powder to get the mirror surface. The coating thickness was examined by measuring average thickness from 5 points using an optical microscope (OM), as shown in Fig 14.

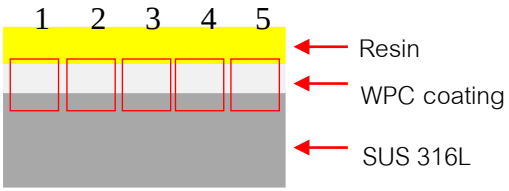

Fig. 14 Measuring points of the coating thickness of the sample

In order to find the proper size of spray nozzle and moving speed of sample pass through spray nozzle, the air pressure from compressor and the spraying distance were controlled at 0.3 MPa and 20 mm, respectively. The SUS 316L substrate was not moved. The three diameter sizes of the spray nozzle, 1.2, 1.7 and 2.0 mm, and the

three moving speeds of sample, 600, 1,200 and 1,800 cm/min were selected to evaluate the appropriate spraying area and apparent of the coating surface.

Figures 15 and 16 show the schematic of the distribution of spray area and the coated surface of specimens from different size of nozzle. From the results, they were found that the size of 1.2 mm diameter of the spray nozzle created the suitable spraying area and the uniform coating surface on the SUS 316L substrate. The nozzle size of 1.2 mm then was used to determine the suitable moving speeds of sample. Coated surfaces of samples from different moving speed are presented in Fig. 17. The coating speed of 600 cm/min condition shows the good result of the surface of coating according to the smooth and uniformity of the coating surface.

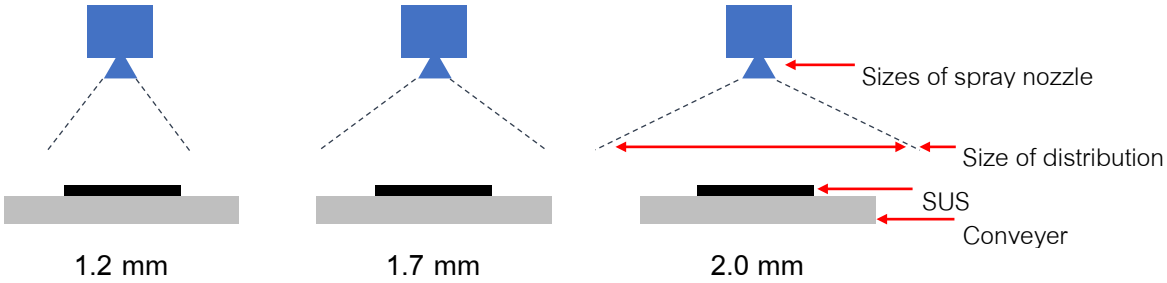

Fig. 15 The distribution of spray area from different size of nozzle

Fig. 16 Coating surface of different size of the spray nozzle

Fig. 17 Coated surface of samples from different moving speed pass through the spray nozzle

Other two parameters that might affect the coating thickness are the coating distance between spray nozzle and sample and the coating repetition. The coating distance of 15, 20, 25 and 30 cm and the coating repetition of 1, 2 and 3 times were selected to conduct. The 100-150 μm coating thickness is the target of this study.

Figures 18-21 show the profiles of the coating thickness along the samples after sprayed on the SUS substrate with different coating distance and repetition. The coating thickness was increased with increasing coating repetition for all coating distance. The coating distance of 15 cm shows a bit over target result after the first time of coating, as shown in Fig. 18.

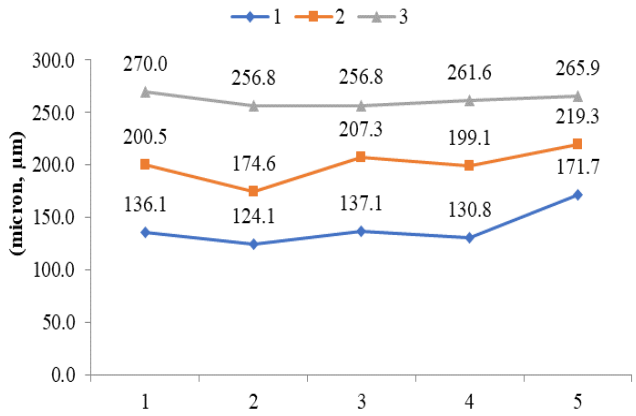

Fig. 18 Coating thickness of samples after sprayed with a coating distances of 15 cm and repetition of 1, 2 and 3 times

The optimum parameters to achieve the coating target were the coating distance of 20 and 25 cm with the repetition for 2-3 times, as shown in Figs. 19 and 20. From the result in Fig. 21, the optimum coating thickness form these conditions (30 cm coating distance, 1-3 spray repetition) was not succeeded.

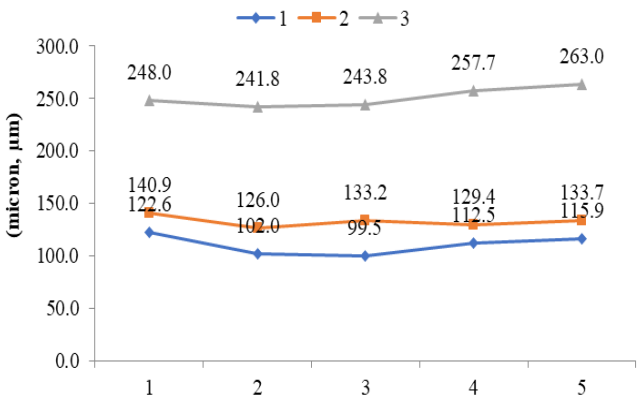

Fig. 19 Coating thickness of samples after sprayed with a coating distances of 20 cm and repetition of 1, 2 and 3 times

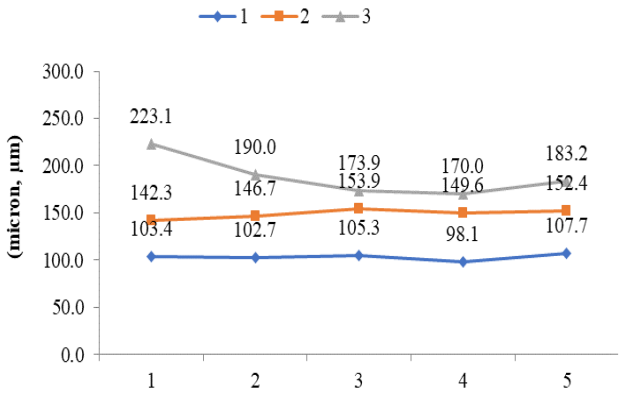

Fig. 20 Coating thickness of samples after sprayed with a coating distances of 25 cm and repetition of 1, 2 and 3 times

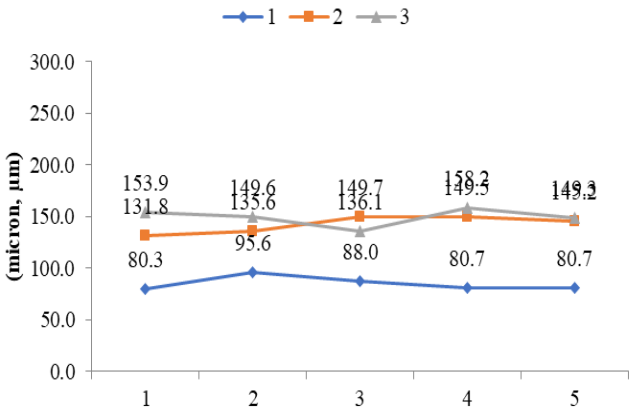

Fig. 21 Coating thickness of samples after sprayed with a coating distances of 30 cm and repetition of 1, 2 and 3 time

The coating thickness results of each coating condition were summarized in Table 7. From the desired thickness of 100-150 µm, the conditions that can be used for preparing the WPC coating sample are as follow: 1. the coating distance of 15 cm and repetition of 1 time (average coating thickness, 139 µm). 2. The coating distance of 20 cm and repetition of 1 and 2 times (average coating thickness, 110 and 132 µm respectively). 3. The coating distance of 25 cm and repetition 1 time (average coating thickness, 103 µm). 4. The coating distance of 30 cm and repetition 2 times (average coating thickness, 142 µm)

From the observation on the coated sample sprayed with the coating distance of 15 cm and 30 cm, the coating surfaces were not be uniform. On the other hand, the samples from the coating distance of 20-25 cm, the surface of the sprayed samples was complete and more consistent. Figure 22 shows the coating layer of the sample coated from the coating distance of 20 cm with 2 times repetition.

Table 7. The coating thickness results of each coating condition

Distance	Repetition	Point of measuring thickness					Mean
		1	2	3	4	5	
30	1	80.3	95.6	88.0	80.7	80.7	85.1
	2	131.8	135.6	149.7	149.5	145.2	142.4
	3	153.9	149.6	136.1	158.2	149.3	149.4
25	1	103.4	102.7	105.3	98.1	107.7	103.4
	2	142.3	146.7	153.9	149.6	152.4	149.0
	3	223.1	190.0	173.9	170.0	183.2	188.0
20	1	122.6	102.0	99.5	112.5	115.9	110.5
	2	140.9	126.0	133.2	129.4	133.7	132.6
	3	248.0	241.8	243.8	257.7	263.0	250.9
15	1	136.1	124.1	137.1	130.8	171.7	139.9
	2	200.5	174.6	207.3	199.1	219.3	200.1
	3	270.0	256.8	256.8	261.6	265.9	262.2

Fig. 22 The coating layer of the sample coated from the coating distance of 20 cm with 2 times repetition

Conclusion

From the results of:

- Raw material preparation and characterization
- The preparation and characterization of HAp/CK and HAp/WPC composite materials
- The development of the novel spray processes coating on stainless-steel substrate and characterization

4 papers were published as attached in appendix.

The study of the HAp/WPC spray coating on stainless-steel substrate and characterization is now under the experiment and developing a manuscript.

Output

1. Weerapol Taptimdee, Prinya Chindaprasirt, Yuichi Otsuka, Yoshiharu Mutoh, **Teerawat Laonapakul**, “Strength and Bioactivity of Hydroxyapatite/White Portland Cement (HAp/WPC) under Simulated Body Fluid (SBF) Solution”, Materials Science Forum, 975, pp. 88-93.

2. Auttachai Jantasang and **Teerawat Laonapakul,** 2019, **“**Cold Spray Parameters for White Portland Cement Coating on Stainless Steel” Research & Knowledge, 5, pp.33-37.

3. **Teerawat Laonapakul**, Ratchawoot Sutthi, Patamaporn Chaikool, Yoshiharu Mutoh, Prinya Chindaprasirt, 2019, “Optimum conditions for preparation of bio-calcium from blood cockle and golden apple snail shell and characterization”, ScienceAsia, 45, pp. 10-20.

4. Ratchawoot Sutthi, Nisanath Kaewwinud, Prinya Chindaprasirt, Yoshiharu Mutoh, **Teerawat Laonapakul**, 2018, “Effect of curing temperature and time on the mechanical properties of hydroxyapatite/calcined kaolin”, ScienceAsia, 44, pp. 397-402.

Appendix

Materials Science Forum
ISSN: 1662-9752, Vol. 975, pp 88-93
doi:10.4028/www.scientific.net/MSF.975.88

Submitted: 2019-06-05
Accepted: 2019-06-18
Online: 2020-01-16

Strength and Bioactivity of Hydroxyapatite/White Portland Cement (HAp/WPC) under Simulated Body Fluid (SBF) Solution

Weerapol Taptimdee[1,a], Prinya Chindaprasirt[2,b], Yuichi Otsuka[3,c], Yoshiharu Mutoh[4,d] and Teerawat Laonapakul[*,1,e]

[1]Department of Industrial Engineering, Faculty of Engineering, Khon Kaen University, Khon Kaen, 40002, Thailand

[2]Sustainable Infrastructure Research and Development Center, Department of Civil Engineering, Faculty of Engineering, Khon Kaen University, Khon Kaen, 40002, Thailand, and, Academy of Science, The Royal Society of Thailand, Dusit, Bangkok, 10300, Thailand

[3]Department of System Safety, Nagaoka University of Technology, Nagaoka, Niigata 940-2188, Japan

[4]Professor Emeritus Nagaoka University of Technology, Nagaoka, Niigata 940-2188, Japan

[a]t.weerapol_noom@hotmail.com, [b]prinya@kku.ac.th, [c]otsuka@vos.nagaokaut.ac.jp, [d]mutohyoshiharu@yahoo.co.jp, [e]teerla@kku.ac.th

Keywords: *in vitro* test, compressive strength, apatite formation

Abstract. In this study, the effects of curing white Portland cement (WPC) and hydroxyapatite mixed with white Portland cement (HAp/WPC) pastes in water and the *in vitro* biological environment on the compressive strength and bone-like apatite formation were examined. The compressive strength of both WPC and HAp/WPC pastes increased with longer curing periods in water. The compressive strength of WPC and HAp/WPC pastes was 51.88 and 25.67 MPa, respectively, after curing in water for 28 days. The compressive strength of both samples continuously increased during *in vitro* testing in a simulated body fluid (SBF). After 4 weeks of immersion in a SBF, the strengths of cured WPC and HAp/WPC samples were 59.01 and 28.06 MPa, respectively. It is due to continued hydration of WPC. The addition of HAp to WPC decreased the compressive strength of the sample. Alternatively, it enhanced bone-like apatite formation on the surface of the samples.

Introduction

A number of substitute materials have been developed as alternatives for bone repair, augmentation and substitution. A bone substitute material often has a negative influence on patients after surgery. It may produce inflammation, infection and incompatibility between the material and the patient. The implications of bone implant materials on the host body are important factors that determines the success or failure of the developed materials. Therefore, a thorough understanding of the correlation between the material properties and biological effects is necessary. A simulated body fluid (SBF) solution has an ion profile and concentration similar to that of human blood plasma. It has been widely applied for *in vitro* evaluations of the artificial bone biomaterial bioactivity. Currently, most of the research studies on bone implant biomaterials use a SBF solution to assess the bioactivity of bone substitute materials by examining bone-like apatite formation on the surfaces of these materials during immersion in the solution [1-3].

Hydroxyapatite (HAp), which has a chemical composition of $Ca_{10}(PO_4)_6(OH)_2$, is one of the calcium phosphate based bioceramics. It has been use in medical and dental applications as a bone substitute material for 30 years since it has excellent biocompatibility, bioactivity and osteoconductive properties as well as chemical and structural similarity to human bone minerals [4]. In various biomedical applications, such as prosthetic and coating implants, HAp is normally used in powder form [5-7]. Unfortunately, the low strength and brittleness of HAp limits its application to only bone repair. White Portland cement (WPC) is the preferred choice to improve the strength of HAp, since its mechanical properties and setting mechanism are similar to those of gray cement. WPC

based materials have been proven non-toxic and feasible for obtaining biocompatibility and bioactivity. They have the potential to promote bone healing and in bone tissue engineering applications. Moreover, WPC has also been shown to be bioactive in bone tissue engineering applications [8-11]. Additionally, the white color of WPC seems makes it a suitable source material for bone substitute materials. While the mechanical properties of bulk HAp have been reported inappropriate in load bearing applications such as orthopedics, HAp/WPC composites are an alternative choice to achieve a favorable combination of properties, and incorporating the best characteristics of each material.

In this study, *in vitro* biological testing of WPC and HAp/WPC samples was conducted in SBF to investigate bone-like apatite formation characteristics. The compressive strengths of both samples before and after bone-like apatite formation were investigated and reported in this work. The compressive strength of samples was determine according to ASTM standards. Bone-like apatite precipitation was investigated using scanning electron microscopy, energy disperse spectroscopy (SEM/EDS) and X-ray diffraction (XRD) techniques.

Materials and Methods

Sample Preparation. The starting materials used in this research were commercial white Portland cement (WPC) and hydroxyapatite (HAp) powders. The WPC powder used in this study had chemical composition consisting of 14.67% SiO_2, 1.93% Al_2O_3, 78.77% CaO, 0.328% Fe_2O_3, 0.31% MgO, 0.04% Na_2O, 3.22% SO_3, and 0.13% TiO. HAp powder was synthesized from calcium carbonate ($CaCO_3$) and dibasic calcium phosphate dehydrate (DCPD) powders using a mechanochemical method [12]. The calcium/phosphorous molar ratio of the mixed powders was 1.67, which is equal to the desired theoretical calcium/phosphorous molar stoichiometry of HAp. In this research, pure WPC (denoted as WPC) powder and mixed of WPC and HAp (denoted as HAp/WPC) powders with a weight ratio of 1:1 were prepared. The mixed powders were blended with distilled water in a solid to liquid ratio of 2:1 by using mechanical mixing machine to prepare pastes of the samples. These pastes were cast into cubic molds (25 mm^3) for compressive strength testing, and disk-shaped molds (diameter 10 mm, 2 mm thick) for bioactivity testing. Then, they were vibrated for 10 seconds to remove entrapped air. All samples were wrapped in plastic sheets to control moisture loss and were stored to set in controlled room at a temperature of 23 °C for 24 hours before testing.

Compressive Strength Testing. After setting under controlled conditions, the cubic paste samples were removed from their molds and then cured in pure water at 23 °C for 3, 7, 14, 21 and 28 days. To stop hydration after curing, the cubic cement samples were immersed into acetone for 1 day and then dried at 40 °C in an incubator. These samples were cured in pure water for 28 days and then they were immersed in SBF for 3, 7, 14, and 28 days. After immersion, the samples were taken out of the solution, gently washed with distilled water and then dried at 40 °C for 24 hours in an incubator. Compressive strength tests were conducted according to ASTM C109 [13] on cubic samples using a hydraulic testing machine at a loading rate of 2 kN/s after curing in water and immersion in SBF solution. The average failure stress values of three samples subjected compressive test were reported for each sample.

Bioactivity Testing. After setting under controlled conditions, disk-shaped paste samples were removed from their molds and cured in pure water at 23 °C for 28 days. These samples were then immersed in a SBF solution at 37 °C for 7 days. The SBF solution had an ion profile and concentration close to that of human blood plasma. It was prepared according to the procedure of Kokubo [14]. After the immersion period, the samples were gently washed with distilled water and dried using blow drier then kept in a desiccator. Bioactivity tests were conducted by observing the formation of bone-like apatite on the sample surfaces. The formation of bone-like apatite and the elemental composition on the sample surface were observed and analyzed using a scanning electron microscope/energy-dispersive X-ray spectroscopy (SEM/EDS, LEO model 1430). The crystalline phases of samples were identified using X-ray diffractometer (XRD, Bruker D8). The XRD analysis

was carried out with CuKα radiation operating at 40 kV and 40 mA at a scanning rate of 2.4° 2θ/min in increments of 0.02°.

Results and Discussion

Compressive Strength Testing.The results of compressive strength development of WPC and HAp/WPC pastes during water curing and during immersion in a SBF solution are shown in Fig.1. As the length of time for water curing was extended, the compressive strength of both types of samples increased (Fig. 1 (a)), as cement hydration was gradually accomplished. When WPC reacted with water, it underwent a hydration process forming ettringite, calcium silicate hydrate and calcium hydroxide, all of which contributed to the strength development seen in the WPC samples [9]. After curing in water for 28 days, the compressive strength achieved by the WPC and HAp/WPC samples was 51.88 and 25.67 MPa, respectively. The addition of HAp to WPC affected the hydration of WPC resulting in a deceased compressive strength. Both of these sample types have potential for use in cancellous bone applications as their compressive strengths are within the range of that of cancellous bone (2-45 MPa) [15].

After curing in water for 28 days, both samples types were immersed in SBF for 3, 7, 14 and 28 days and then subjected to compression testing. The results are shown in Fig. 1 (b). It can be seen from this figure that the compressive strength of WPC and HAp/WPC samples gradually increased to 59.02 and 28.06 MPa, respectively, after four weeks of immersion in SBF solution. The increased strength of WPC after immersion in SBF solution may have been due to continued hydration of the samples. The increasing compressive strength of the WPC samples was greater than that of HAp/WPC samples based on the purity of WPC. However, the increased strength of these specimens after immersion in SBF solution is a good indicator that they can be used as a bone substitute material for implantation in a physiological environment.

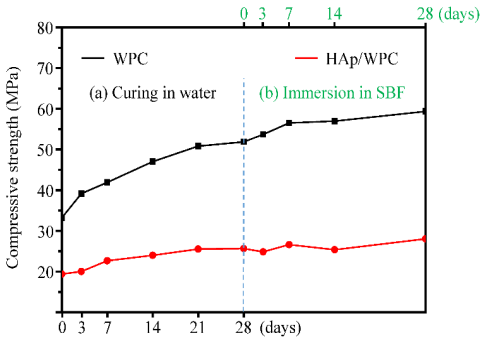

Fig.1 Compressive strength of the WPC and HAp/WPC samples

Bioactivity testing. Fig. 2 shows the XRD patterns of the as-cured WPC and HAp/WPC samples and those of these samples after immersion in SBF solution for 7 days. The XRD patterns of the as-cured WPC and HAp/WPC samples are shown in Fig. 2 (a). The major crystalline phases detected in both samples were calcite, portlandite and ettringite, which are the crystalline phases found in hydrated cement. Excluding the crystalline phases of hydrated cement, the characteristic peaks of the HAp phase were detected on the HAp/WPC sample due to the addition of HAp during the sample preparation. The XRD patterns of the WPC and HAp/WPC samples after immersion in SBF solution for 7 days are shown in Fig. 2 (b). Changes in the phase composition of both samples were observed. The peak intensity of the portlandite phase disappeared after 7 days of immersion, whereas those of calcite and ettringite phases decreased after immersion in SBF solution for 7 days. From the results, it can be concluded that these three phases dissolved in the SBF solution.

An increasingly broad peak intensity of a HAp phase was observed at about 2θ = 25.8° and 31-33° on WPC samples after 7 days of immersion, as shown from Fig. 2 (b). The peak intensity of the HAp phase of HAp/WPC changed its appearance from a sharp to broad peak intensity after 7 days of

immersion. These results implied that the amorphous phase of bone-like apatite was precipitated on the surfaces of both samples. The composition of the dissolved of phase of WPC increased the degree of supersaturation in the SBF solution by increasing the ionic activity of apatite and accelerated bone-like apatite nucleation on the surfaces [16].

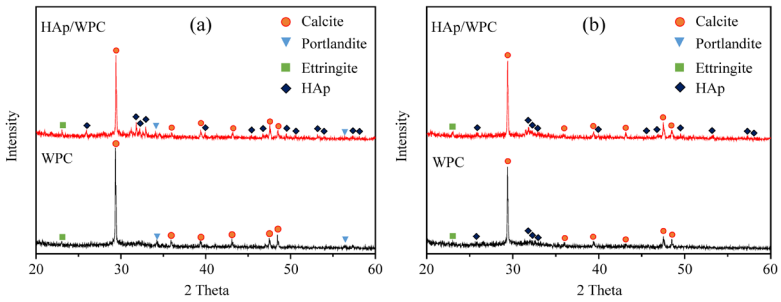

Fig. 2 XRD patterns of samples (a) as-cured and (b) after immersion in SBF for 7 days for WPC and HAp/WPC

Fig. 3 shows the morphological changes observed on the as-cured WPC and HAp/WPC sample surfaces. Fig. 3 (a) displays a homogeneous structure showing the compacted surface of the WPC sample before immersion. Irregularly shaped WPC particles were observed on its surface. For the HAp/WPC before immersion, irregularly shaped WPC particles were mixed with round HAp particles as shown in Fig. 3 (b). EDS analysis of the WPC and HAp/WPC surfaces before immersion in the SBF solution are shown in Fig. 3 (c) and (d), respectively. The presence of calcium (Ca), silicon (Si), magnesium (Mg) and aluminum (Al) was observed. An aurum (Au) peak intensity was detected due to the Au coating applied prior to SEM observations. Phosphorus (P) was detected on the HAp/WPC surfaces due to the HAp present in this type of sample. A low intensity peak of P was detected and was difficult to observe due to the small amounts of phosphate compounds. The peak intensity of P was nearly equal to that of Au.

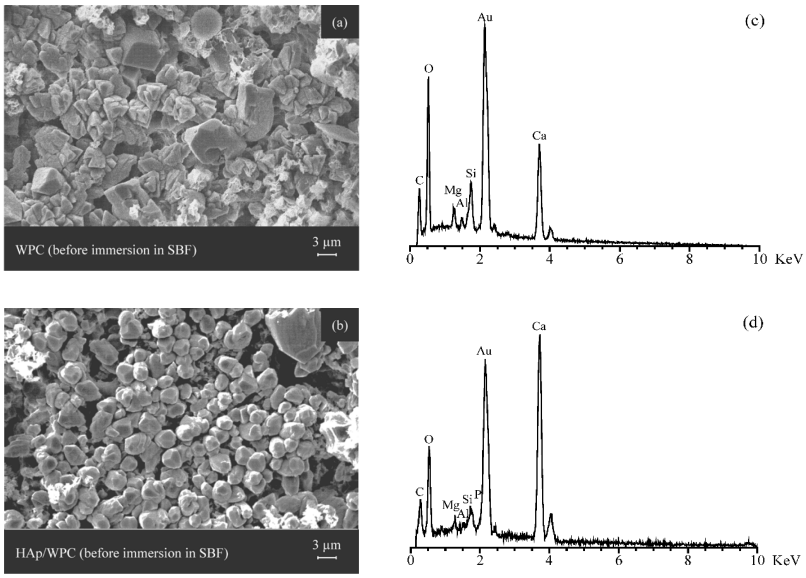

Fig. 3 SEM/EDS micrograph showing morphological changes on sample surfaces of the as-cured WPC and HAp/WPC samples: (a) SEM micrograph of the WPC sample, (b) SEM micrograph of the HAp/WPC sample (c) EDS analysis of the WPC sample, and, (d) EDS analysis of the HAp/WPC sample

Fig. 4 shows the morphological changes of WPC and HAp/WPC surfaces after immersion in SBF solution for 7 days. The surface texture of the WPC and HAp/WPC samples changed so that it had highly porous surfaces with tiny spherical particles, as presented in Fig. 4 (a) and (b). The spherical

particles on the HAp/WPC surfaces were larger than those on the WPC surfaces. Fig. 4 (c) and (d) show the EDS spectra of the WPC and HAp/WPC surfaces after immersion in SBF solution for 7 days. A high intensity peak of the P spectrum was clearly observed in addition the Ca, Si and Mg spectra. A stronger intensity peak of P spectrum was observed in the HAp mixed sample. The SEM observations, EDS and XRD analysis confirmed precipitation of a bone-like apatite on the WPC and HAp/WPC sample surfaces during immersion in the SBF solution.

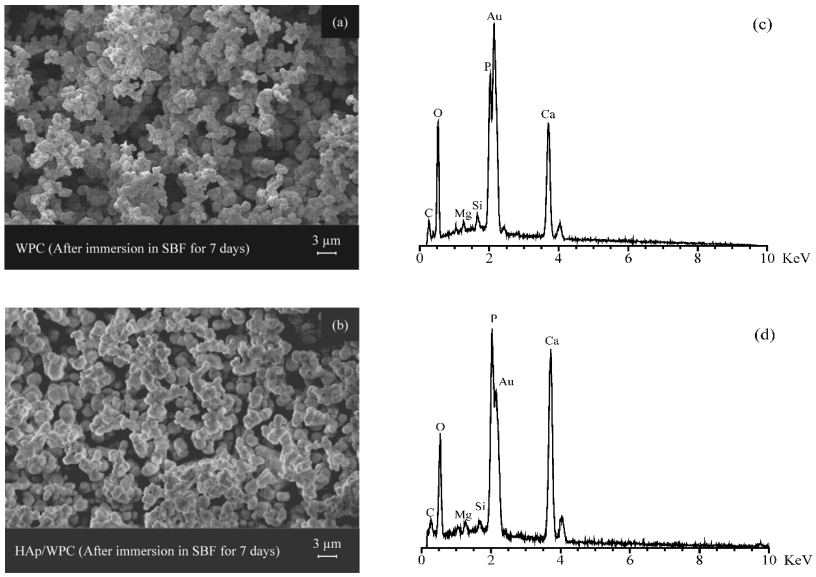

Fig. 4 SEM/EDS of surface morphological changes of WPC and HAp/WPC after immersion in SBF solution for 7 days: (a) SEM micrograph of a WPC sample, (b) SEM micrograph of a HAp/WPC sample, (c) EDS analysis of a WPC sample, and, (d) EDS analysis of a HAp/WPC sample

Conclusions

The effects of hydroxyapatite mixed with white Portland cement on the compressive strength and bioactivity of these samples after immersion in an *in vitro* environment (containing SBF) were examined. It can be concluded that:

1. The compressive strength of WPC and HAp/WPC increased continuously during *in vitro* testing.
2. Addition of HAp to WPC decreased the compressive strength of these samples. After 28 days of immersion in a SBF solution, the compressive strengths of the WPC and HAp/WPC samples were 59.02 and 28.06 MPa, respectively.
3. Addition of HAp into WPC samples improved bone-like apatite formation on the surfaces of the samples.

Acknowledgements

This research was supported by the Thailand Research Fund and the Office of the Higher Education Commission [Grant No. MRG6180026] and the Capacity Building Program for New Researcher 2018 from National Research Council of Thailand (NRCT). The second author would like to acknowledge the support of Thailand Research Fund (TRF) under the TRF Distinguished Research Professor Grant No. DPG6180002. The last author would like to acknowledge support of the Supply Chain and Logistics System Research Unit, Faculty of Engineering, Khon Kaen University, Thailand.

References

[1] Y. W. Gu, K. A. Khor, and P. Cheang: Biomaterials Vol. 24 (2003), p. 1603-1611
[2] Y. W. Gu, K. A. Khor, D. Pan, and P. Cheang: Biomaterials Vol. 25 (2004), p. 3177-3185
[3] X. Lu and Y. Leng : Biomaterials Vol. 26 (2005), p. 1097-1108
[4] G. J. Meijer, J. Heethaar, M. S. Cune, C. De Putter, and C. A. Van Blitterswijk: Int. J. Oral Maxillofac. Surg. Vol. 26 (1997), p. 135-140
[5] B. Kundu, M. K. Sinha, M. K. Mitra, and D. Basu: Bull. Mater. Sci. Vol. 27 (2004), p. 133-140
[6] S. Kold, O. Rahbek, M. Vestermark, S. Overgaard, and K. Søballe: J. Arthroplasty Vol. 21 (2006), p. 263-270
[7] P. Chandran, M. Azzabi, J. Miles, M. Andrews, and J. Bradley: J. Arthroplasty Vol. 25 (2010), p. 52-57
[8] D. Gallego, N. Higuita, F. Garcia, N. Ferrell, and D. J. Hansford: Mater. Sci. Eng. C Vol. 28 (2008), p. 347-352
[9] N. J. Coleman, J. W. Nicholson, and K. Awosanya: Cem. Concr. Res. Vol. 37 (2007), p. 1518-1523
[10] P. Torkittikul and A. Chaipanich: Mater. Sci. Eng. C Vol. 32 (2012), p. 282-289
[11] S. Pangdaeng, V. Sata, J. B. Aguiar, F. Pacheco-Torgal, and P. Chindaprasirt: Mater. Sci. Eng. C Vol. 51 (2015), p. 1-6
[12] R. Sutthi, S. Pangdaeng, P. Chindaprasirt, Y. Otsuka, Y. Mutoh, and T. Laonapakul: Key Eng. Mater. Vol. 718 (2016), p. 133-138
[13] "Standard Test Method for Compressive Strength of Hydraulic Cement Mortars (Using2-in. or [50-mm] Cube Specimens)," Annu. B. ASTM Standard
[14] T. Kokubo and H. Takadama: Biomaterials Vol. 27 (2006), p. 2907-2915
[15] G. Hannink and J. J. C. Arts: Injury Vol. 42 (2011), p. S22-S25
[16] S. M. Salman, S. N. Salama, H. Darwish, and H. A. Abo-Mosallam: Ceram. Int. Vol. 35 (2009), p. 1083-1093

Vol. 5 No. 1 page 33-37
DOI : 10.14456/randk.2019.6

RESEARCH & KNOWLEDGE

Research Article

Cold Spray Parameters for White Portland Cement Coating on Stainless Steel

Auttachai Jantasang[1] and Teerawat Laonapakul[1*]

[1]Department of Industrial Engineering, Faculty of Engineering, Khon Kean University

Abstract: This research aims to study parameters that affect white Portland cement coating on 316L stainless steel using the cold spray technique in order to achieve 100-150 μm of coating thickness. The evaluation parameters, which were studied are: 1) speed of the sample moving pass through the spray nozzle 2) size of the spray nozzle 3) distance between the coating nozzle and sample surface 4) coating repetition. After the cold spray process, the thickness of the specimen was analyzed using an optical microscope. From preliminary experiments, the results showed that the nozzle of 1.2 mm with the speed of the sample moving pass through the nozzle of 600 cm/min produced good surface condition and satisfying distribution of coating area on coated sample. In addition, a distance between the nozzle of 20 cm with twice coating times, was the optimum condition created 132 μm of coating thickness of the coated sample.

Keywords: White Portland cement, Stainless steel costing, Cold spray

1. Introduction

The stainless steel grade 316L is material that is widely used in surgery due to its good corrosion resistant and the ability to be compatible with human tissue (Gopi et al, 2013). However, the stainless steels may corrode inside the body under certain circumstances in a highly stressed and oxygen depleted region, such as the contacts under the screws of the bone fracture plate. Therefore, this material is suitable to use only in temporary implant devices. To improve their bioactivity, stainless steel is usually coated with hydroxyapatite (HAp), which has been widely used in medical applications due to their favorable biocompatibility and osteoconductivity (Baptista et al 2016, Dey et al, 2009). Therefore, a bioactive HAp coating on stainless steel surface would be one of the most promising implant materials of a good combination of coating biocompatibility and substrate strength. The plasma spraying is now widely accepted method for HAp coating because it gives tight adhesion between HAp and metal substrate with a coating thickness about 100 to 150 μm. Unfortunately, disadvantages of the plasma spray process are relative high cost and complexity of process. Moreover, the extremely high temperature of plasma spray is cause of decomposition of the coating, instability of coating-substrate interface, thermal expansion mismatch, residual stress in coating layer and unstable duration of coating under body fluids and varying local loading (Ishikawa, et al., 1997; Lu et al, 2004). Therefore, novel cold spray coating is an interesting technology need to be studied to obtain surface coating. This technique may offer several technological advantages over thermal spray, for examples, tensile residual stress, thermal decomposition and instability of coating-substrate interface may be avoided. However, the formation of HAp coating on the metal substrate at low temperature is a limitation. In order to solve this restriction, White Portland cement (WPC) is the prefer choice to study since its setting behavior and strength development are essentially the same as that expected in gray cement. WPC based materials have been proved non-toxic and feasibility of obtaining biocompatibility and bioactivity. It has potential to promote bone healing and bone tissue engineering application. Moreover, WPC has also been proved the feasibility of obtaining bioactivity for bone tissue engineering application (Chaipanich and Torkittikul, 2011; Gallego, et al. 2008; Coleman, et al. 2007; Abdullah, et al. 2002; Torkittikul and Chaipanich, 2009; Torkittikul and Chaipanich, 2012; Pangdaeng et al., 2015.). In addition, white color of WPC seems to be suitable source material for bone substitute materials.

The principal objective of this study to develop the novel spray tool and process of WPC coating on stainless-steel substrate and to evaluate the optimum parameters to achieve the coating thickness at 100 - 150 μm. The evaluation parameters, which were studied are: 1) spray nozzle size 2) speed of the sample moving pass through the spray nozzle 3) distances between coating nozzle and sample surface 4) coating repetition.

* Corresponding Author: teerla@kku.ac.th, +66 859 160 505

2. Materials and Methods

2.1 Materials preparation

The materials used in the research are stainless steel 316L (SUS 316L) plate and commercial grade white Portland cement (WPC). The chemical composition of WPC is shown in Table 1. The SUS 316L plate was cut to a shape of rectangular with a size of 10x20x3 mm. They were then sand-blasted in order to get average roughness (Ra) of 3-6 μm (Dey et al, 2009). The blasted plates were then washed in acetone for 30 minutes using ultrasonic machine to remove grease and remaining sand on the samples. The WPC powder was sifted through a 100-mesh screen and then mixed with distilled water at a ratio of 1: 0.5 by weight before spraying.

2.2 Spray coating parameters and sample preparation

Figure 1 shows schematic design of cold spray coating equipment, which is compose of: 1) air compressor 2) spray gun with three different sizes of nozzle and 3) coating table, which can adjust the speed of sample moving and coating distance. In this study, four spraying parameters were selected to study the suitable coating condition for achieving optimum coating thickness of 100-150 μm, as follow: 1) sizes of the spray nozzle of 1.2, 1.7 and 2.0 mm. 2) speeds of sample moving pass through the spray nozzle of 600, 1,200 and 1,800 cm/min 3) distances between the spray nozzle and sample of 15, 20, 25 and 30 cm. and 4) coating repetition of 1, 2 and 3 times. For each condition, the air pressure from compressor was fix at appropriate pressure of 0.3 MPa.

Table. 1 Elements of Portland Cement White. (Pangdaeng et al., 2015.)

Material	Chemical composition (%)							
	SiO_2	Al_2O_3	CaO	Fe_2O_3	MgO	Na_2O	SO_3	TiO
WPC	14.68	1.93	78.77	0.33	0.31	0.04	3.22	0.12

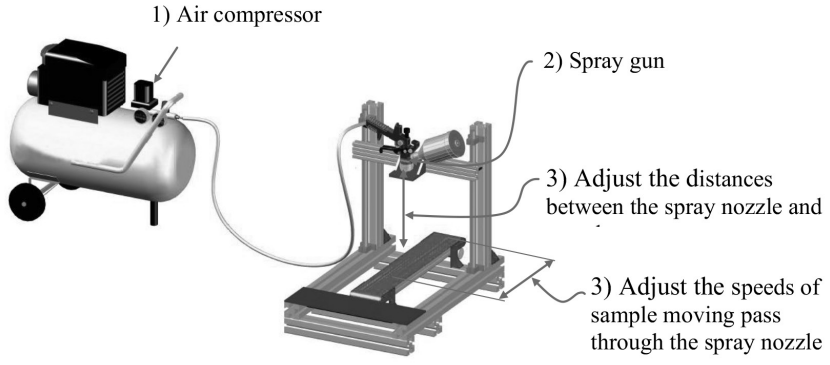

Fig. 1 Schematic design of cold spray coating equipment

After spraying, the coated samples were leaved at ambient temperature for 1 hour and cured in water for 24 hours to allow the coating layer setting. The coated samples were then mounted into resin and allowed them to solidify at room temperature for 24 hours. The mounted samples were polished with sandpaper and diamond powder to get the mirror surface. The coating thickness was examined by measuring average thickness from 5 points using an optical microscope (OM), as shown in Fig 2.

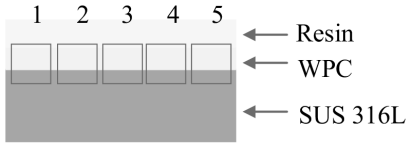

Fig. 2 Measuring points of the coating thickness of the sample

3. Results and discussion

3.1 The size of the spray nozzle and moving speed of sample pass through the spray nozzle

In order to find the proper size of spray nozzle, the air pressure from compressor and the spraying distance were controlled at 0.3 MPa and 20 mm, respectively. The SUS 316L substrate was not moved. The three diameter sizes of the spray nozzle, 1.2, 1.7 and 2.0 mm were selected to evaluate the appropriate spraying area. After selected a proper nozzle size, the three moving speeds of sample, 600, 1,200 and 1,800 cm/min were selected to evaluate the good speed condition for spraying.

Figures 3 and 4 show the schematic of the distribution of spray area and the coated surface of specimens from different size of nozzle, respectively. From the results, they were found that the size of 1.2 mm diameter of the spray nozzle created the suitable spraying area and the uniform coating surface on the SUS 316L substrate. The nozzle size of 1.2 mm then was used to determine the suitable moving speeds of sample. Coated surfaces of samples from different moving speed are presented in Fig. 5. The coating speed of 600 cm/min condition shows the good result of the surface of coating according to the smooth and uniformity of the coated surface.

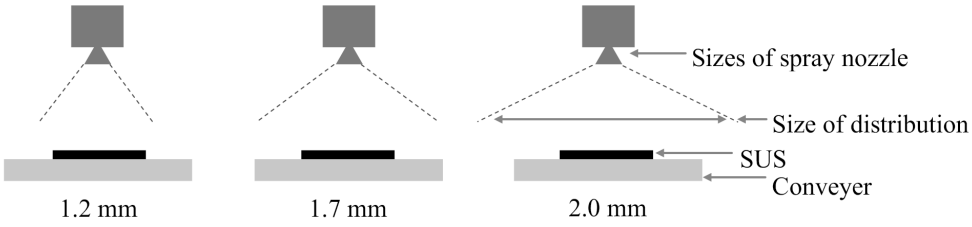

Fig.3 The distribution of spray area from different size of nozzle

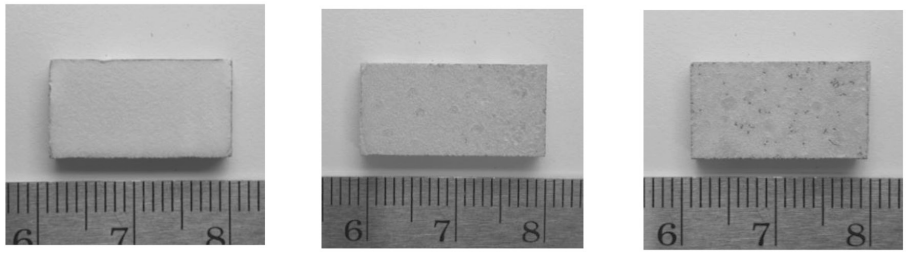

Fig. 4 Coating surface of different size of the spray nozzle.

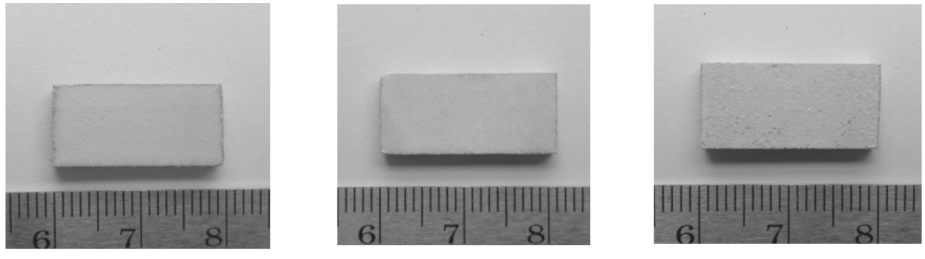

Fig. 5 Coated surface of samples from different moving speed pass through the spray nozzle

3.2 The coating distances between spray nozzle and sample and the coating repetition

Other two parameters that might affect the coating thickness are the coating distance between spray nozzle and sample and the coating repetition. The coating distance of 15, 20, 25 and 30 cm and the coating repetition of 1, 2 and 3 times were selected to conduct. The 100-150 μm coating thickness is the target of this study.

Figures 6-9 show the profiles of the coating thickness along the samples after sprayed on the SUS substrate with different coating distance and repetition. The coating thickness was increased with increasing coating repetition for all coating distance. The coating distance of 15 cm shows a bit over target result after the first time of coating, as shown in Fig. 6.

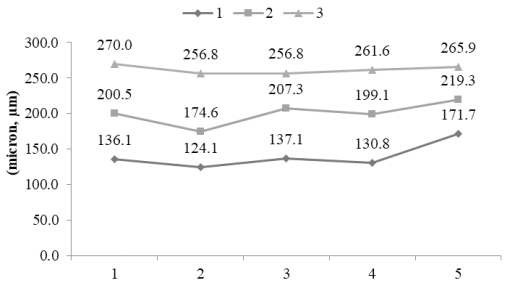

Fig. 6 Coating thickness of samples after sprayed with a coating distances of 15 cm and repetition of 1, 2 and 3 times

The optimum parameters to achieve the coating target were the coating distance of 20 and 25 cm with the repetition for 1-2 times, as shown in Figs. 7 and 8.

From the result in Fig. 9, the optimum coating thickness form these conditions (30 cm coating distance, 1-3 spray repetition) was not success.

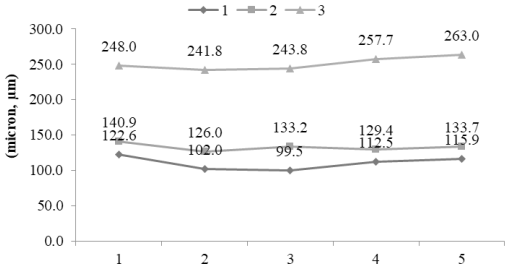

Fig. 7 Coating thickness of samples after sprayed with a coating distances of 20 cm and repetition of 1, 2 and 3 times

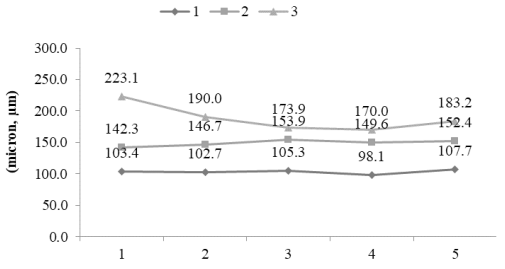

Fig 8. Coating thickness of samples after sprayed with a coating distances of 25 cm and repetition of 1, 2 and 3 times.

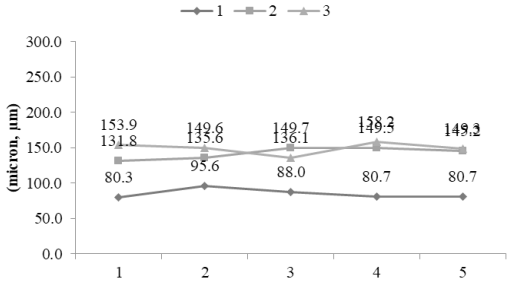

Fig 9. Coating thickness of samples after sprayed with a coating distances of 30 cm and repetition of 1, 2 and 3 times.

The coating thickness results of each coating condition were summarized in Table 2. From the desired thickness of 100-150 µm, the conditions that can be used for preparing the WPC coating sample are as follow: 1. the coating distance of 15 cm and repetition of 1 time (average coating thickness, 139 µm). 2. The coating distance of 20 cm and repetition of 1 and 2 times (average coating thickness, 110 and 132 µm respectively). 3. The coating distance of 25 cm and repetition 1 time (average coating thickness, 103 µm). 4. The coating distance of 30 cm and repetition 2 times (average coating thickness, 142 µm)

From the observation on the coated sample sprayed with the coating distance of 15 and 30 cm, the coating surfaces were not be uniform. On the other hand, the samples from the coating distance of 20 and 25 cm, the surface of the sprayed samples was completion and more consistency when compared to those sprayed with the coating distance of 15 and 30 cm. Figure 10 shows the coating layer of the sample coated from the coating distance of 20 cm with 2 times repetition.

4. Conclusion

The cold spray and processes of WPC coating on stainless-steel substrate were developed. The optimum parameters to achieve the coating thickness of 100-150 µm were summarized as follow:

Table 2 The coating thickness results from each coating condition

Distance	Repetition	Point of measuring thickness					Mean
		1	2	3	4	5	
30	1	80.3	95.6	88.0	80.7	80.7	85.1
	2	131.8	135.6	149.7	149.5	145.2	142.4
	3	153.9	149.6	136.1	158.2	149.3	149.4
25	1	103.4	102.7	105.3	98.1	107.7	103.4
	2	142.3	146.7	153.9	149.6	152.4	149.0
	3	223.1	190.0	173.9	170.0	183.2	188.0
20	1	122.6	102.0	99.5	112.5	115.9	110.5
	2	140.9	126.0	133.2	129.4	133.7	132.6
	3	248.0	241.8	243.8	257.7	263.0	250.9
15	1	136.1	124.1	137.1	130.8	171.7	139.9
	2	200.5	174.6	207.3	199.1	219.3	200.1
	3	270.0	256.8	256.8	261.6	265.9	262.2

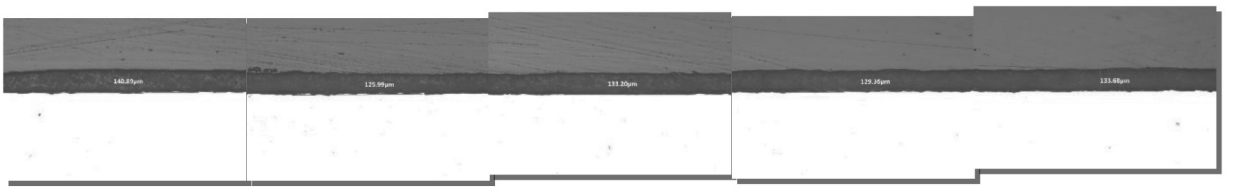

Fig 10. The coating layer of the sample coated from the coating distance of 20 cm with 2 times repetition

1. The nozzle size of 1.2 mm and coating speed of 600 cm/min created the suitable distribution of spray area with uniform coating surface on the SUS substrate.

2. The optimum parameters to achieve the coating target were the coating distance of 20 and 25 cm with the repetition for 2-3 times. The coating distance of 20 cm with 2 times repetition has an average thickness 132μm which is the desired thickness range (100-150μm).

3. The coating thickness increased with decreasing the coating distance and increasing the spraying repletion.

5. Acknowledgement

This research was supported by the Supply Chain and Logistics System Research Unit, Faculty of Engineering, Khon Kaen University, Thailand. The last author would like to acknowledge the support of the Thailand Research Fund and the Office of the Higher Education Commission [Grant No. MRG6180026] and the Capacity Building Program for New Researcher 2018 from National Research Council of Thailand.

6. Reference

Abdullah, D., et al. (2002). An evaluation of accelerated Portland cement as a restorative material, *Biomaterials*, vol. 23(19), October 2002, pp. 4001–4010.

Baptista. R., et al. (2016). Characterization of titanium-hydroxyapatite biocomposites processed by dip coating, *Materials Science,* vol. 39(1), February 2016, pp. 263–272.

Chaipanich, A., and Torkittikul, P. (2011). Microstructure: Surface and cross-sectional studies of hydroxyapatite formation on the surface of white Portland cement paste in vitro, *Applied Surface Science*, vol. 257(20), August 2011, pp. 8385-8390.

Coleman, N., et al. (2007). A preliminary investigation of the in vitro bioactivity of white Portland cement, *Cement and Concrete Research*, vol. 37, November 2007, pp. 1518–1523.

Dey, A., et al. (2009). Characterization of microplasma sprayed hydroxyapatite coating, *Thermal Spray Technology,* vol. 18(4), December 2009, pp. 578–592.

Gallego, D., et al. (2008). Bioactive coatings on Portland cement substrates: Surface precipitation of apatite-like crystals, *Materials Science and Engineering C,* vol. 28(3), April 2008, pp. 347–352.

Gopi, J., et al. (2013). Hydroxyapatite Coating on Selectively Passivated and Sensitively Polymer-Protected Surgical Grade Stainless Steel, *Applied Electrochemistry,* vol. 43(8), March 2013, pp. 331–345.

Ishikawa, K., et al. (1997). Blast coating method: New method of coating titanium surface with hydroxyapatite at room temperature, *Biomedical Materials Research*, vol. 38(2), February 1997, pp. 129-134.

Lu, Y., et al. (2004). Plasma-sprayed hydroxyapatite + titania composite bond coat for hydroxyapatite coating on titanium substrates, *Biomaterials,* vol. 25(18), August 2004, pp. 4393-4403.

Pangdaeng, S., et al. (2015), Apatite formation on calcined kaolin–white Portland cement geopolymer, *Materials Science and Engineering C*, vol. 51, June 2015, pp. 1-6.

Torkittikul, P. and Chaipanich, A. (2009). Investigation of the mechanical and in vitro biological properties of ordinary and white Portland cements, *Science Asia*, vol. 35(4), December 2009, pp. 358–364.

Torkittikul, P. and Chaipanich, A. (2012). Optimization of calcium chloride content on bioactivity and mechanical properties of white Portland cement, *Materials Science and Engineering C*, vol.32(2), March 2012, pp. 282-289.

RESEARCH ARTICLE
doi: 10.2306/scienceasia1513-1874.2019.45.010

ScienceAsia 45 (2019): **10–20**

Optimum conditions for preparation of bio-calcium from blood cockle and golden apple snail shells and characterization

Teerawat Laonapakul[a,*], **Ratchawoot Sutthi**[a], **Patamaporn Chaikool**[b], **Yoshiharu Mutoh**[c], **Prinya Chindaprasirt**[d,e]

[a] Department of Industrial Engineering, Faculty of Engineering, Khon Kaen University, Khon Kaen 40002 Thailand
[b] Department of Mechanical Engineering, Faculty of Engineering, Rajamangala University of Technology Isan Khon Kaen Campus, Khon Kaen 40000 Thailand
[c] Nagaoka University of Technology, Nagaoka, Niigata 940-2188 Japan
[d] Sustainable Infrastructure Research and Development Centre, Department of Civil Engineering, Faculty of Engineering, Khon Kaen University, Khon Kaen 40002 Thailand
[e] Academy of Science, the Royal Society of Thailand, Bangkok 10300 Thailand

*Corresponding author, e-mail: teerla@kku.ac.th

Received 6 May 2018
Accepted 27 Feb 2019

ABSTRACT: Research on the utilization of calcium compounds from seashells has attracted much interest in diverse applications. However, the optimum temperature and time for preparation of calcium compounds from shells remains unknown. These factors have a direct effect on the purity of the obtained calcium phases. In this study, the influence of calcination temperature and holding time on the phase transformations of $CaCO_3$ from sea shells and freshwater shells, i.e., blood cockle and golden apple snail shells, was studied. High purity and crystalline $CaCO_3$ and CaO was produced from both types of shells by calcination at 600 °C and 800 °C, respectively. Overall both blood cockle and golden apple snail shells could be used to produce calcium compounds with 95–98% pure calcium with trace amounts of As, Cd, Hg, and Pb. Phase transformation of $CaCO_3$ depends on calcination temperature and holding time. The calcium content in $CaCO_3$ and CaO from golden apple snail shells was higher than that from blood cockle shells. This result also indicated that the calcium compounds from blood cockle shell were easier to grind than those from golden apple snail shells primarily due to an early transformation of the calcium phase of golden apple snail shells.

KEYWORDS: $CaCO_3$, CaO, phase transformations, calcination

INTRODUCTION

Blood cockles (*Anadara granosa*) are a type of bivalve mollusc, which are commonly found at muddy seashores. Blood cockle farming is quite extensive on the eastern and southern coasts of Thailand. The annual production of blood cockles in Thailand between 2009 and 2016 ranged from 40–81 thousand tonnes[1]. It is one of the most popular seafoods in Thailand and is a good protein source. Golden apple snails (*Pomacca canaliculata*) are very serious invasive freshwater pests. They cause damage to agricultural products, especially rice and aquatic plants, leading to huge economic losses[2]. It has been estimated that in Thailand, golden apple snails cause losses of at least 3000 million US dollars annually[3]. Nonetheless, they have been used as a protein source in animal feeds and human foods[4–7]. The large consumption of blood cockle and golden apple snails results in a considerable amount of shell by-products that is now treated as waste.

The three common mineral forms found in various sea shells are the aragonite, calcite and vaterite phases of $CaCO_3$. These shells are composed of 97–99% of $CaCO_3$ with some minor compounds, viz., MgO, Al_2O_3, Fe_2O_3, SiO_2, $Ca_3P_2O_8$, $CaSO_4$, proteins and mucopolysaccharides. Additionally, trace amounts of Sn, Mo, Mn, Cd, Ti, B, Pb, Au, Ag, Ni, Co, Bi, Cu, Sr, Rb and As are present[8]. Another source of calcium, CaO, is obtained from the calcination of limestone or $CaCO_3$[9,10]. Normally, dolomite, limestone and magnesite from sedimentary rocks are the common natural sources for the production of $CaCO_3$ and CaO. Nevertheless, large scale mining

of raw materials, such as limestone, results in extensive deforestation and top soil loss. This contributes to environmental damage and the high costs for environmental compliance incurred.

Nowadays, research on the utilization of calcium compounds from seashells has attracted much interest. Numerous studies have been done with the aim of using alternative sources of $CaCO_3$ and CaO from various sea shells. This calcium has been widely used in diverse applications. It is notable that this approach uses shell by-products in an economically feasible manner and has the environmental benefits of waste recovery. For example, $CaCO_3$ from oyster, mussel, cockle, clam and bivalve shells has been applied as fillers in environmentally friendly thermoplastic composites[11–13], substitute materials in the production of plastering cement and construction materials[14–16], suitably used in plant fertilizer and as reagents for efficient phosphate removal from wastewater[17,18] and in biomimetic designs of ceramic/polymer and ceramic/polymer/-fibre composites[19]. Additionally, $CaCO_3$ extracted from blood cockle shells has been used as a biomaterial for tissue engineering applications, drug delivery systems, bone tissue and bone grafts[20–22]. $CaCO_3$ can be prepared from shells with and without calcination. A temperature of 500 °C with various holding times from 15 min to 5 h was used to produce $CaCO_3$. CaO obtained from the calcination of shells has been used in various applications such as a renewable catalyst for biodiesel production[23–25], a material to absorb CO_2 for air cleaning applications[26,27] and an initial substrate to produce hydroxyapatite ceramic biomaterials[28]. Various calcination temperatures from 600 °C to 1000 °C with holding times from 30 min to 4 h were applied to shells to obtain CaO. Insufficient information exists about the influence of calcination temperature and holding time on the phase transformations of $CaCO_3$ in shells that have a direct effect on the purity of the $CaCO_3$ and CaO phases.

In the present study, transformations of the calcium phase of seawater blood cockle and fresh water golden apple snail shells were studied. Calcination temperatures ranging from 600 °C to 900 °C with 1–4 h holding periods were used to investigate the effects of these parameters on their transformation and elemental composition. This information will be useful in understanding of the effects of calcination temperature and holding time. Effective calcination method to obtain the required calcium compounds from shells could thus be developed.

MATERIALS AND METHODS

Material preparation

The blood cockle (BC) shells used in this study were collected from seafood restaurants in Khon Kaen province. These restaurants are supplied by producers from the coastal areas of Eastern Thailand. Golden apple snail (GAS) shells were collected from paddy fields in Khon Kaen province, Thailand. First, the collected GAS shells were broken into pieces with sizes similar to those of BC shell, the average size of shell was 3×4 cm^2. The broken GAS and the BC shells were then cleaned with a brush in tap water to remove dirt and then boiled in hot water for 20 min. After cleaning, they were air-dried for 24 h and oven-dried at 60 °C for another 24 h. The prepared shells were stored in a desiccator at a room temperature of 25–29 °C.

Material characterization

To study the weight loss and thermal behaviour of these calcium products, the prepared shells were separately crushed into fine powders using a porcelain mortar and pestle. Thermogravimetric analysis at ambient temperature (25–29 °C) to 1100 °C at a heating rate of 5 °C/min under an O_2 atmosphere was done on the samples using a thermogravimetric analyser/differential scanning calorimeter (TGA/DSC1, Mettler).

To study the influence of calcination temperature and holding period on the transformation of the crystalline phases in BC and GAS shells, the prepared shells were separately calcined at four different temperatures, viz., 600, 700, 800, and 900 °C for 1, 2, 3, and 4 h using a heating rate of 5 °C/min. After calcination, they were crushed in a porcelain mortar into fine powders. The crystalline phase composition of these powders was investigated using X-ray diffraction (XRD, Bruker D8) at a scan rate of 2.4° 2θ/min in 0.02° 2θ increments with CuKα radiation. The elemental composition of raw shells and shells calcined at 600, 700, 800, and 900 °C for 1 h were determined using wavelength dispersive X-ray fluorescence (WDXRF, Axios mAX). Microstructural observations of shell samples were carried out using scanning electron microscopy (SEM, LEO 1450). 100 g of shell samples calcined for 1 h were ground and analysed for their particle size distributions using a particle size analyser (HORIBA, LA-950). The trace (heavy metal) elements (As, Cd, Hg, and Pb) in shell powders were also analysed using inductively coupled plasma/mass spectroscopy (ICP/MS, AGILENT 7500C).

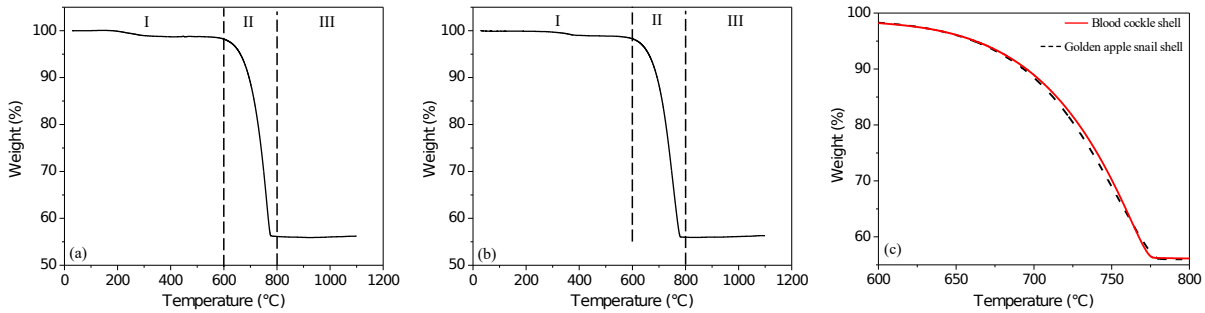

Fig. 1 TGA patterns of (a) blood cockle shell, (b) golden apple snail shell, and (c) blood cockle and golden apple snail shells between 600 and 800 °C.

RESULTS AND DISCUSSION

Thermogravimetric analysis of shells

Fig. 1 shows the results of thermogravimetric a
sis (TGA) of shell samples. The TGA curves fo
types of shells were similar to three distinct s
of weight loss, as shown in Fig. 1a,b. In the
stage (I) at temperatures below 600 °C, the w
of both shell samples decreased slightly by 2
In the second stage (II) at temperatures bet
600 and 800 °C, the weights decreased rapidly
they had lost 44% of their weight. In the
stage (III) at temperatures above 800 °C, the w
of shell samples remained almost constant. F
shows a comparison of shell weight losses in
II. The weight loss of BC shell was slightly s
than that of GAS shell. From the results, calcir
temperatures of 600, 700, 800, and 900 °C were selected to investigate the changes in elemental composition and transformation of the crystalline phases of shells. To study the influence of holding period on phase transformation, four different holding times, 1, 2, 3, and 4 h, were used.

Transformation of the crystalline phases during calcination

The XRD patterns of raw BC and GAS shells are shown in Fig. 2. The broad peak patterns of both shells corresponded to an amorphous (poorly crystallized) aragonite phase of $CaCO_3$. This is in agreement with previous reports of the presence of an aragonite phase in bivalve shells[29] and cockle shells[30].

Figs. 3 and 4 show XRD patterns of shells after calcination at temperatures of 600, 700, 800, and 900 °C and 1–4 h holding times. The XRD patterns of both shells calcined at 600 °C at all holding periods showed only the sharp characteristic peaks of a calcite phase, as shown in Figs. 3a and 4a.

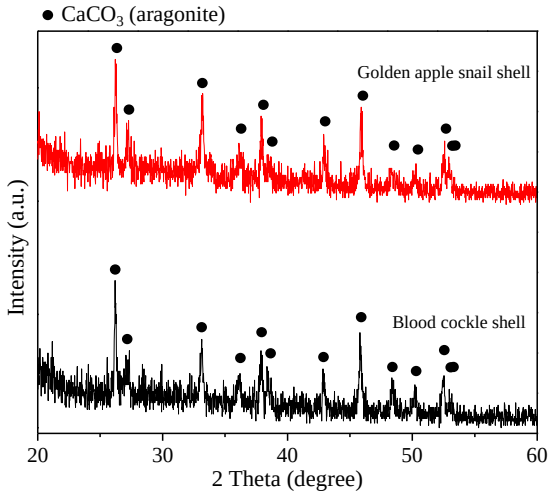

Fig. 2 XRD patterns of raw blood cockle and golden apple snail shells.

For the samples calcined at 700 °C, the single sharp characteristic peaks of a calcite phase was observed for BC shells after a holding period of 1–3 h and for GAS shells after a holding period of 1–2 h, as depicted in Figs. 3b and 4b. This finding is in good agreement with previous XRD results for patterns of aragonite and calcite of $CaCO_3$[31]. The initial stage of weight loss observed in TGA analysis was due to the removal of water from shells and phase transformation of amorphous aragonite into crystalline calcite. Bischoff[32] reported that this transformation occurred at low temperatures due to the instability of the aragonite phase. For the BC shells calcined at 700 °C for 4 h and 800 °C for 1 h, as well as the GAS shells calcined at 700 °C for 3 and 4 h, calcite co-existed with CaO as shown in Figs. 3b,c and 4b. This suggests that the phase transformation of $CaCO_3$ to CaO started at a temperature between 700

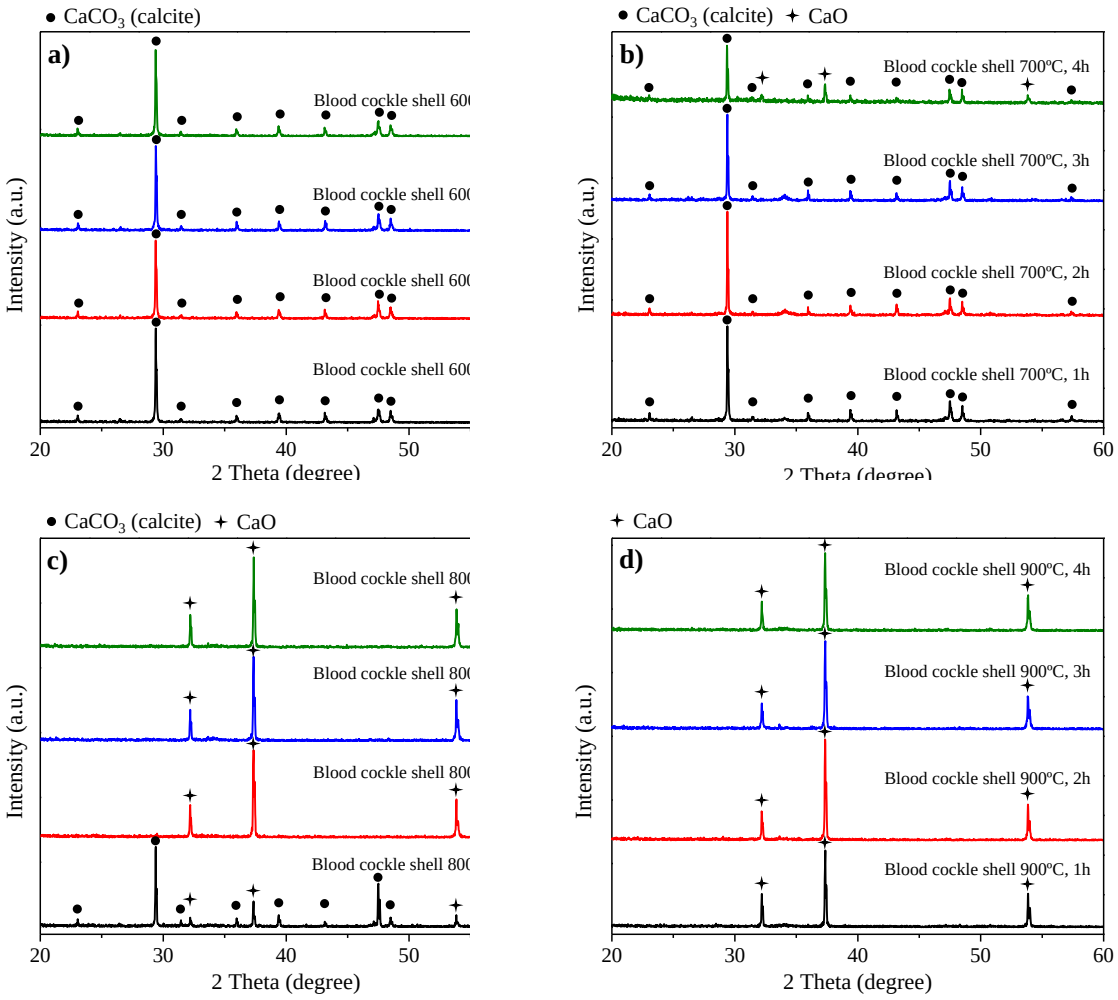

Fig. 3 XRD patterns of blood cockle shell after calcination at (a) 600 °C, (b) 700 °C, (c) 800 °C, and (d) 900 °C for various holding times.

and 800 °C. The characteristic peaks associated with complete disappearance of the $CaCO_3$ phase after calcination at 800 °C for 2 h for the BC shells and after all holding durations at 800 °C for GAS shells, are shown in Figs. 3c and 4c. The phase change in the BC shells was slower than for the GAS shells since the BC shells were thicker. This result is consistent with TGA analysis showing that the weight loss of the BC shells was slightly slower than for the GAS shells. When the calcination temperature was 900 °C for all holding periods, only the characteristic peaks associated with CaO phase were observed, as shown in Figs. 3d and 4d. This result indicated that amorphous $CaCO_3$ (aragonite) was completely transformed to crystalline $CaCO_3$ (calcite) and CaO at temperatures of 600 °C and 800 °C, respectively. The XRD results thus indicated that both calcination temperature and holding time were important for the phase transformation of $CaCO_3$ in both shells.

Surface morphology observation during calcination

The surface morphologies of raw shells and calcined shells at 600, 700, 800, and 900 °C for 1 h were observed under SEM and the results are shown in Figs. 5–7. The surfaces of BC shells contained parallel cleavages (Fig. 5a) similar to a prismatic structure with prominent and uniformly distributed pores. The structure was well connected and composed of fine grains (approximately 2 μm) of calcium compounds, (Fig. 5b). Alternatively, the surface of GAS shells was relatively smooth (Fig. 5c) consisting of small compact and connected homogeneous fine grains (approximately 1 μm) of calcium

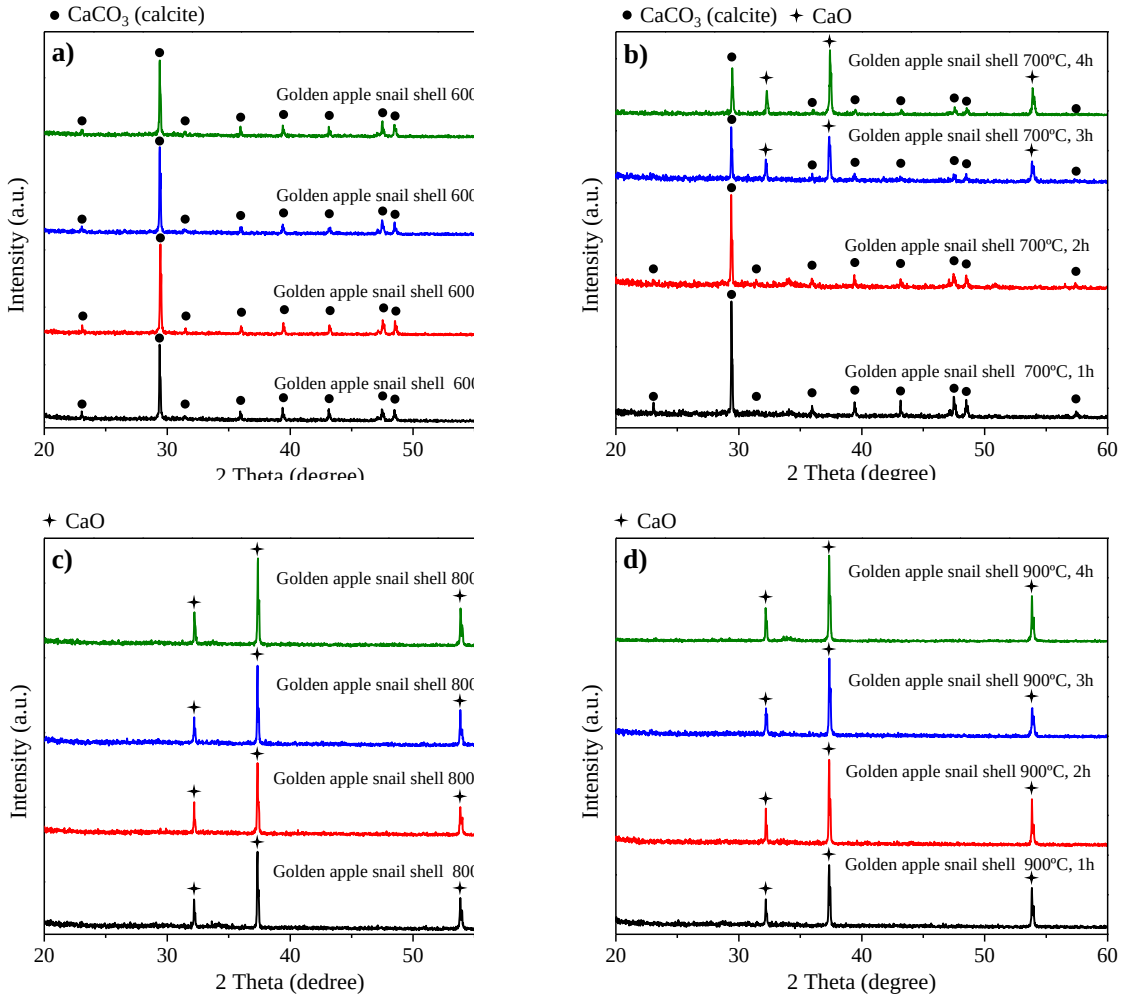

Fig. 4 XRD patterns of golden apple snail shell after calcination at (a) 600 °C, (b) 700 °C, (c) 800 °C, and (d) 900 °C for various holding times.

compounds (Fig. 5d).

Figs. 6 and 7 show scanning electron micrographs of shells that were calcined at 600, 700, 800, and 900 °C for 1 h. After calcination at 600 °C, the surface morphologies of both shell types changed quite noticeably. In the BC shell, the parallel cleavages were not present. Both shells showed non-uniform irregular surfaces consisting of units up to 10–15 μm, as shown in Figs. 6a and 7a. The surface showed an agglomerated phase of a sintered matrix that was due to the removal of water and organic material from the raw shells. The amorphous aragonite phase of $CaCO_3$ in raw shells was transformed into a crystalline calcite phase of $CaCO_3$ after calcination at 600 °C. This finding concurs with the results of XRD analysis. After calcination at 700 °C, the surfaces became more uniform with the presence of many small units (approximately 3–5 μm) of a calcium compound, as shown in Figs. 6b and 7b. In these figures, the microstructure of both raw shells calcined at high temperatures of 800 and 900 °C were markedly different from the shells calcined at 600 and 700 °C. Increasing the temperature to 800 °C and 900 °C resulted in the formation of uniform micro-granules and fine grains (approximately 3–5 μm) of calcium compounds, as shown in Figs. 6c,d and 7c,d. This change in surface morphology resulted from a transformation of the calcite phase of $CaCO_3$ to CaO, releasing CO_2 during high temperature calcination. The surface densities of GAS shell were higher than those of BC shells at all calcination temperatures.

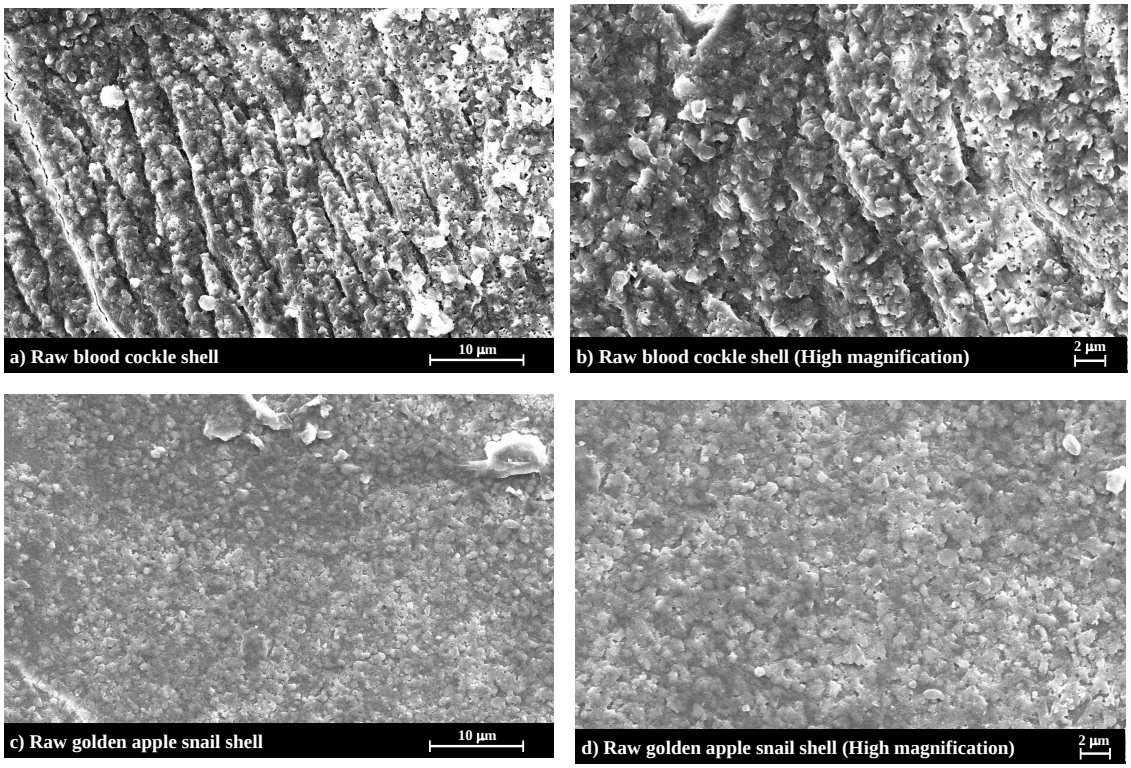

Fig. 5 SEM micrographs of surface morphology of (a) raw blood cockle shell, (b) high magnification of raw blood cockle shell, (c) raw golden apple snail shell, and (d) high magnification of raw golden apple snail shell.

Elemental composition in shells during calcination

The elemental composition of raw and calcined BC and GAS shell powders at all calcination temperatures for 1 h was determined using X-ray fluorescence. The results presented in Table 1 show that raw BC and GAS shells were comprised of 93% and 93% CaO by weight, respectively. These findings show that a high amount of calcium was present in both shells. Other minor elements, viz., Na, Sr, Cl, Si, Mg, S, Fe, Al, K, Mn, P, and Ba, were also present and their levels decreased with increasing calcination temperature. Awang-Hazmi[33] and Bharatham[34] studied the mineral and physiochemical properties of raw cockle and molluscan shells and their potential for use as a biomaterial for bone repair. They found that cockle shells contain more than 90% calcium. This finding is similar to reported literature values. Other elements present were Na, Mg, P, K, Fe, Cu, Ni, B, Zn, and Si. The proportion of CaO in BC and GAS shells calcined at 900 °C was 97% and 98%, respectively. This was higher than that of those shells calcined at 600 °C, 95%, and 96%, respectively. The calcium content of GAS shells was higher than that of BC shells. This result is mainly due to a higher content of Na_2O in BC shells. The influence of environmental factors (seawater and freshwater) affects the composition of shells in surficial sediment[35]. The large amount of CaO is associated with the presence of calcium compounds, which was confirmed by the XRD results. The XRF and XRD analysis indicated that highly pure $CaCO_3$ and CaO can be produced from BC and GAS shells.

Grindability of $CaCO_3$ and CaO

$CaCO_3$ (calcite) was obtained after calcination of shells at 600 °C for 1 h, while CaO was obtained after calcination at 900 °C for same time. The shells calcined at 600 and 900 °C for 1 h were used to test material grindability. 100 g of each type of calcined shell was manually ground for 10 min in a porcelain mortar using a pestle. The particle size distribution of shell powders was characterized using a particle size analyser (HORIBA, LA 950). Fig. 8 presents the particle size distributions of these shells. The BC shells showed finer particles than the GAS shells. For shells calcined at 600 °C, the

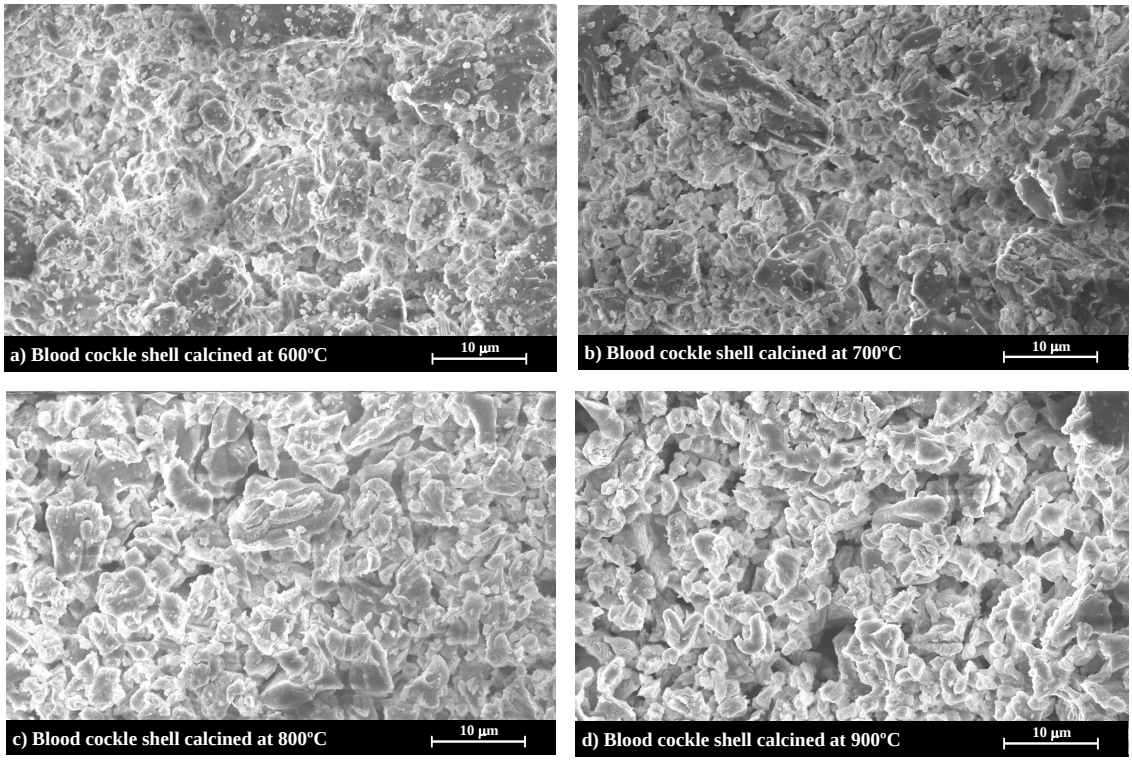

Fig. 6 SEM micrographs of surface morphology of blood cockle shell after calcination at (a) 600 °C, (b) 700 °C, (c) 800 °C, and (d) 900 °C.

Table 1 Elemental composition of raw and calcined blood cockle and golden apple snail shells calcined for 1 h.

Element	Blood cockle shell (%w)					Golden apple snail shell (%w)				
	Raw	600 °C	700 °C	800 °C	900 °C	Raw	600 °C	700 °C	800 °C	900 °C
CaO	93.23	95.43	95.45	95.98	97.19	93.26	96.22	96.81	96.90	98.29
Na_2O	3.77	2.67	2.91	2.20	1.64	1.75	1.40	1.46	1.29	0.77
SrO	0.52	0.04	0.41	0.42	0.39	0.28	0.19	0.27	0.25	0.25
Cl	0.49	0.43	0.35	0.21	0.20	0.37	0.60	0.38	0.27	0.19
SiO_2	0.35	0.40	0.28	0.17	0.14	2.33	0.53	0.23	0.18	0.10
MgO	0.21	0.22	0.16	0.13	0.13	0.16	0.24	0.18	0.12	0.06
SO_3	0.13	0.12	0.11	0.08	0.08	0.22	0.09	0.07	0.06	0.04
Fe_2O_3	0.13	0.14	0.09	0.06	0.06	0.12	0.10	0.06	0.05	–
Al_2O_3	0.12	0.30	0.10	0.05	0.06	1.10	0.20	0.20	0.05	0.07
K_2O	0.79	0.05	0.06	0.59	0.08	0.05	0.06	0.03	0.52	–
MnO	0.05	0.04	0.05	–	–	0.07	0.08	0.08	0.08	0.08
P_2O_5	0.03	0.03	0.02	–	0.02	0.04	–	0.03	0.03	–
BaO	0.16	0.12	–	0.11	–	0.23	0.29	0.18	0.20	0.14

average particle sizes of BC and GAS shells were 7 and 10 µm, respectively. These values were 22 and 30 µm, respectively, for shells calcined at 900 °C. The particle size of shells calcined at 900 °C was greater than that of 600 °C due to the increased hardness of CaO obtained from a higher calcination temperature. This result indicates that the calcium compounds obtained from BC shells were easier to grind than those of GAS shells. The GAS shells were slightly more difficult to grind as a result of continue heating after the phase change was completed due to the early transformation of the calcium phase and the surface density of the calcined shells.

Scanning electron micrographs of $CaCO_3$ (cal-

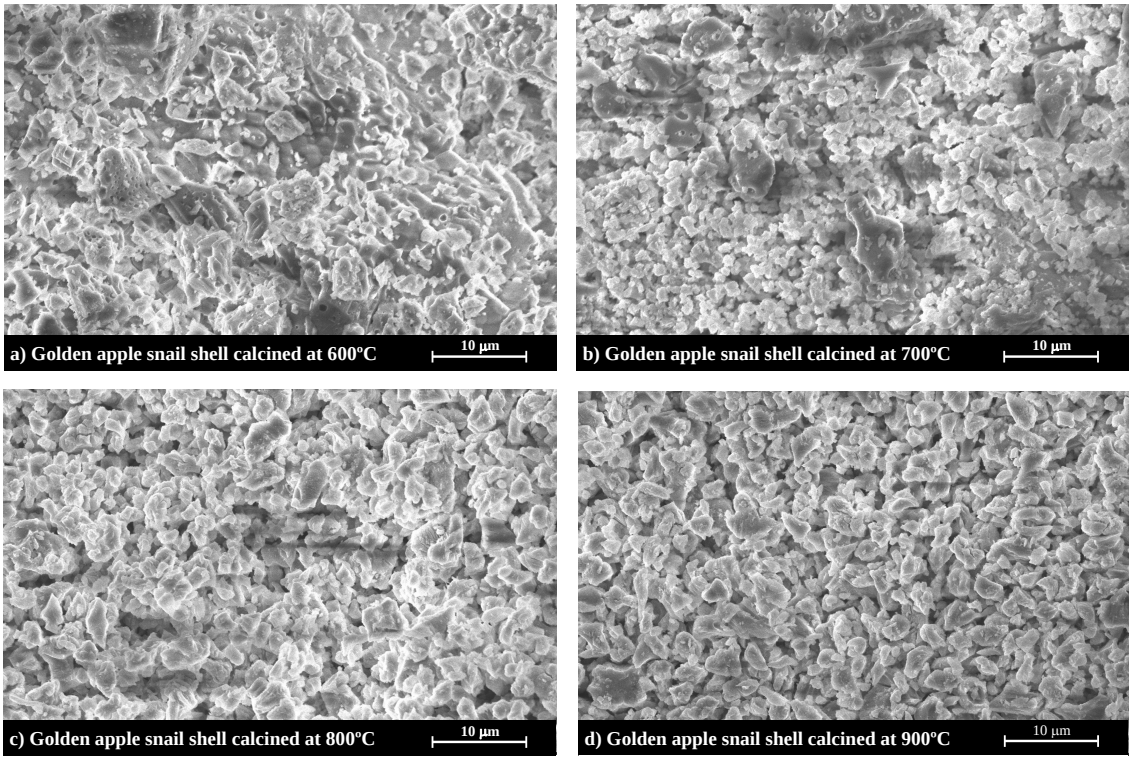

Fig. 7 SEM micrographs of surface morphology of golden apple snail shell after calcination at (a) 600 °C, (b) 700 °C, (c) 800 °C, and (d) 900 °C.

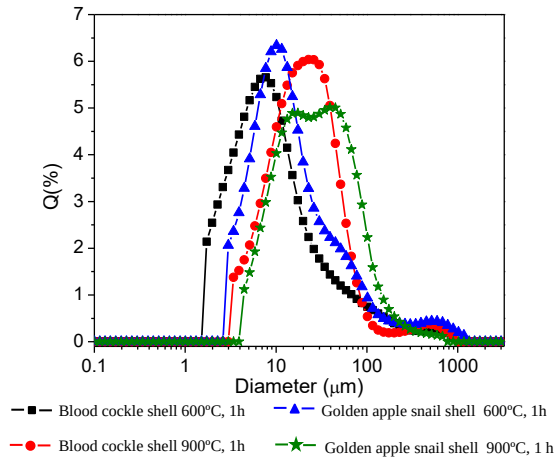

Fig. 8 Particle size distribution of blood cockle and golden apple snail shells after calcination at 600 °C and 900 °C.

cite) and CaO from shells are shown in Fig. 9. The SEM micrographs of $CaCO_3$ (calcite) (Fig. 9a,b) show highly crystallized particles with dense surfaces and irregular morphology. The morphology of CaO was different than $CaCO_3$. For CaO, small round particles were agglomerated at the surfaces, as shown in Fig. 9c,d.

Trace (heavy metal) element in blood cockle and golden apple snail shells

Many products, especially pharmaceutical materials and those for surgical implants[36,37] (e.g., hydroxyapatite and beta tricalcium phosphate) require materials that are relatively free of heavy metal elements. Further investigation of the amount of As, Cd, Hg, and Pb heavy metal elements was thus required. The presence of elements was quantitatively determined using inductively coupled plasma/mass spectroscopy on shell powders. The results, (Table 2), indicate that the amounts of these elements in both raw and calcined shells (600 and 900 °C) are very low. Neither BC nor GAS shells contained As, Cd, Hg, or Pb concentrations exceeding the levels established by ASTM F1185-03 and ASTM F1108-04a required for ceramic hydroxyapatite and beta tricalcium phosphate for surgical implants derived from natural sources. These results are in agreement with a study on cockle and three other shells for used as a material for bone implants[34]. The levels

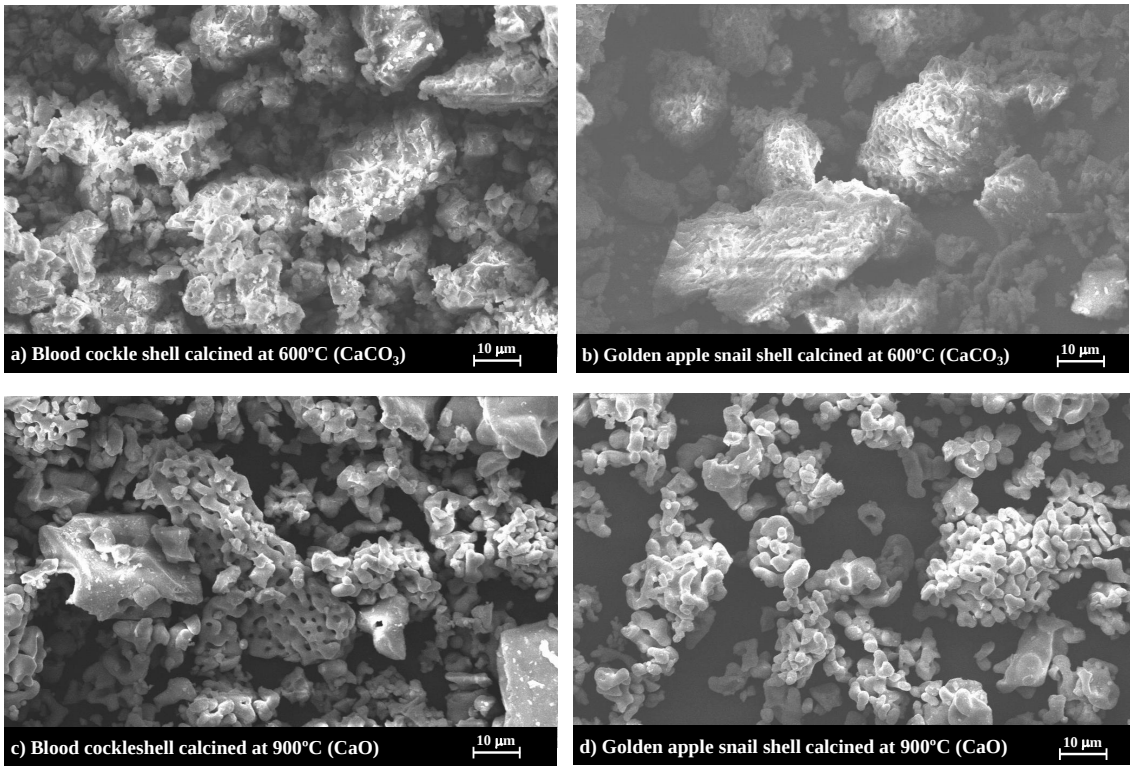

Fig. 9 SEM micrographs of $CaCO_3$ (calcite) powders from (a) blood cockle shell, (b) golden apple snail shell, and CaO powders from (c) blood cockle shell, and (d) golden apple snail shell.

Table 2 Concentrations of heavy metal element in raw and calcined blood cockle and golden apple snail shells at 600 and 900 °C for 1 h.

Element	Blood cockle shell (ppm)			Golden apple snail shell (ppm)			ASTM standard[†]
	Raw	600 °C	900 °C	Raw	600 °C	900 °C	(ppm)
Arsenic (As)	0.093	0.881	0.533	0.049	0.137	0.145	5
Cadmium (Cd)	ND[†]	0.032	0.051	ND	ND	ND	3
Lead (Pb)	0.219	0.633	0.399	0.065	0.056	0.051	30
Mercury (Hg)	ND	ND	ND	ND	ND	ND	5

[†] ASTM F1185-03 and ASTM F1108-04a; ND = Not Detected.

of heavy metal elements in BC shells were higher than those in GAS shells. This may result from the influence of environmental factors. Seawater can be highly polluted as a result of domestic and industrial wastewater discharge, sea traffic, accidents and wastewater from port services.

CONCLUSIONS

The influences of calcination temperature and holding time on the transformation of the crystalline phases in seawater blood cockle and fresh water golden apple snail shells were investigated. The elemental composition, heavy metal element content and physical characterization of both shells were determined. The main conclusions are as follows.

(1) Thermal gravimetric and XRD analyses showed three distinct stages of crystalline phase transformation in both shells. In Stage I, weight of shells slightly decreased during heating from ambient temperature to 600 °C. An amorphous aragonite phase of $CaCO_3$ was transformed into a crystalline calcite phase of $CaCO_3$. In Stage II, the weight of shells rapidly decreased in the temperature range of 600–800 °C. Here, the calcite phase of $CaCO_3$ was transformed into CaO. In Stage III, weight of shells was constant at temperatures higher than 800 °C. At

this point, $CaCO_3$ in shells were completely transformed into CaO. Both calcination temperature and holding time were important for the phase transformation of $CaCO_3$ in each of these shell types. The phase transformation in golden apple snail shells was faster than that of blood cockle shells due to the thickness of their shells.

(2) The elemental composition of blood cockle and golden apple snail shells can be altered by calcination. Fine particle and highly crystalline $CaCO_3$ (calcite) and CaO with some minor elements, Na, Sr, Cl, Si, Mg, S, Fe, Al, K, Mn, P, and Ba, can be produced from blood cockle and golden apple snail shells. The calcium content in the form of $CaCO_3$ and CaO from fresh water golden apple snail shells was higher than that of seawater blood cockle shells. The influence of environmental factors (seawater and freshwater) may have affected the chemical composition of the shell products.

(3) The average particle size of calcium compounds ($CaCO_3$ and CaO) obtained from blood cockle shells was finer than from golden apple snail shells by about 3–8 μm. This resulted from continued heating after the phase transformation of calcium in golden apple snail shells and the surface morphology of these shells.

(4) The content of heavy metal elements (As, Cd, Hg, and Pb) found in raw and calcined blood cockle and golden apple snail shells was much less than the requirements of ASTM standard specifications for producing ceramic hydroxyapatite and beta tricalcium phosphate for surgical implants.

Acknowledgements: This study was financially supported by the Faculty of Engineering, Khon Kaen University, Thailand. P.C. is immensely grateful to the Thailand Research Fund (TRF) for the support under the TRF Distinguished Research Professor Programme, Grant No. DPG6180002. T.L. would like to acknowledge the support of the Thailand Research Fund and the Office of the Higher Education Commission, Grant No. MRG6180026 and the Farm Engineering and Automatic Control Technology Research Group (FEAT), Khon Kaen University, Thailand.

REFERENCES

1. Department of Fisheries, Ministry of Agriculture and Cooperatives Thailand (2016) Statistic of Marine Shellfish Culture Survey 2016. www.fisheries.go.th/strategy-stat/themeWeb/books/2559/1/yearbook_2559.pdf. [Accessed 15 Jan 2018]
2. Thaewnon-Ngiw B, Klinbunga S, Phanwichien K, Sangduen N, Lauhachinda N, Menasveta P (2004) Genetic diversity and molecular markers in introduced and Thai native apple snails (*Pomacea* and *Pila*). *J Biochem Mol Biol* **37**, 493–502.
3. Chaichana R, Sumpan T (2014) The potential ecological impact of the exotic snail Pomacea canaliculata on the Thai native snail *Pila scutata*. *ScienceAsia* **40**, 11–5.
4. Bombeo-Tuburan I, Fukumoto S, Rodriguez E (1995) Use of the golden apple snail, cassava, and maize as feeds for the tiger shrimp, *Penaeus monodon*, in ponds. *Aquaculture* **131**, 91–100.
5. Jintasataporn O, Tabthipwon P, Yenmark S (2004) Substitution of golden apple snail meal for fishmeal in Giant Freshwater Prawn, *Macrobrachium rosenbergii* (de Man) diets. *Kasetsart J* **38**, 66–71.
6. Rattanaporn K, Iuanloy W, Ieng-ubol S, Songsioon W and Chimsung N (2006) Effect of molasses on golden apple snail silage production. *Kasetsart J* **40**, 135-40.
7. Da CT, Lundh T, Lindberg JE (2012) Evaluation of local feed resources as alternatives to fish meal in terms of growth performance, feed utilisation and biological indices of striped catfish (*Pangasianodon hypophthalmus*) fingerlings. *Aquaculture* **364**, 150–6.
8. Narasimhulu KV, Rao JL (2000) EPR and IR spectral studies of the sea water mussel Mytilus conradinus shells. *Spectrochim Acta A Mol Biomol Spectrosc* **56**, 1345–53.
9. Rodriguez-Navarro C, Ruiz-Agudo E, Luque A, Rodriguez-Navarro AB, Ortega-Huertas M (2009) Thermal decomposition of calcite: Mechanisms of formation and textural evolution of CaO nanocrystals. *Am Mineral* **94**, 578–93.
10. Escardino A, Garcia-Ten J, Saburit A, Feliu C, Gómez-Tena MP (2013) Calcium carbonate decomposition in white-body tiles during firing in the presence of carbon dioxide. *Ceram Int* **39**, 6379–90.
11. Tongamp W, Kano J, Zhang QW, Saito F (2008) Simultaneous treatment of PVC and oyster-shell wastes by mechanochemical means. *Waste Manage* **28**, 484–8.
12. Thumsorn S, Yamada K, Leong YW, Hamada H (2011) Development of cockleshell-derived $CaCO_3$ for flame retardancy of recycled PET/recycled PP blend. *Mater Sci Appl* **2**, 59–69.
13. Hamester MRR, Balzer PS, Becker D (2012) Characterization of calcium carbonate obtained from oyster and mussel shells and incorporation in polypropylene. *Materials Res* **15**, 204–8.
14. Yoon GL, Kim BT, Kim BO, Han SH (2003) Chemical-mechanical characteristics of crushed oyster-shell. *Waste Manage* **23**, 825–34.
15. Lertwattanaruk P, Makul N, Siripattarapravat C (2012) Utilization of ground waste seashells in cement mortars for masonry and plastering. *J Environ Manage* **111**, 133–41.
16. Djobo JNY, Tchakouté HK, Ranjbar N, Elimbi A, Tchadjié LN, Njopwouo D (2016) Gel composition

and strength properties of alkali-activated oyster shell-volcanic ash: effect of synthesis conditions. *J Am Ceram Soc* **99**, 3159–66.
17. Kwon HB, Lee CW, Jun BS, Weon SY, Koopman B (2004) Recycling waste oyster shells for eutrophication control. *Resour Conserv Recy* **41**, 75–82.
18. Barros MC, Bello PM, Bao M, Torrado JJ (2009) From waste to commodity: transforming shells into high purity calcium carbonate. *J Clean Prod* **17**, 400–7.
19. Chen B, Peng X, Wang JG, Wu X (2004) Laminated microstructure of Bivalva shell and research of biomimetic ceramic/polymer composite. *Ceram Int* **30**, 2011–4.
20. Hoque ME, Shehryar M, Nurul-Islam KM (2013) Processing and characterization of cockle shell calcium carbonate ($CaCO_3$) bioceramic for potential application in bone tissue engineering. *J Mater Sci Eng* **2**, 1–5.
21. Putro JN, Handoyo N, Kristiani V, Soenjaya SA, Ki OL, Soetaredjo FE, Ju YH, Ismadji S (2014) *Pomacea sp* shell to hydroxyapatite using the ultrasound-microwave method (U-M). *Ceram Int* **40**, 11453–6.
22. Lertcumfu N, Jaita P, Manotham S, Jarupoom P, Eitssayeam S, Pengpat K, Rujijanagul G (2016) Properties of calcium phosphates ceramic composites derived from natural materials. *Ceram Int* **42**, 10638–44.
23. Viriya-empikul N, Krasae P, Puttasawat B, Yoosuk B, Chollacoop N, Faungnawakij K (2010) Waste shells of mollusk and egg as biodiesel production catalysts. *Bioresour Technol* **101**, 3765–7.
24. Buasri A, Chaiyut N, Loryuenyong V, Worawanitchaphong P, Trongyong S (2013) Calcium oxide derived from waste shells of mussel, cockle, and scallop as the heterogeneous catalyst for biodiesel production. *Sci World J* **2013**, 460923.
25. Lesbani A, Tamba P, Mohadi R, Fahmariyanti F (2013) Preparation of calcium oxide from *Achatina fulica* as catalyst for production of biodiesel from waste cooking oil. *Indo J Chem* **13**, 176–80.
26. Li YJ, Zhao CS, Chen HC, Duan LB, Chen XP (2009) CO_2 capture behavior of shell during calcination/carbonation cycles. *Chem Eng Technol* **32**, 1176–82.
27. Ma KW, Teng H (2010) CaO powders from oyster shells for efficient CO_2 capture in multiple carbonation cycles. *J Am Ceram Soc* **93**, 221–7.
28. Zhou H, Yang M, Zhang M, Hou S, Kong S, Yang L, Deng L (2016) Preparation of Chinese mystery snail shells derived hydroxyapatite with different morphology using condensed phosphate sources. *Ceram Int* **42**, 16671–6.
29. Yang W, Kashani N, Li XW, Zhang GP, Meyers MA (2011) Structural characterization and mechanical behavior of a bivalve shell (*Saxidomus purpuratus*). *Mater Sci Eng C* **31**, 724–9.
30. Islam KN, Bakar MZBA, Ali ME, Hussein MZB, Noordin MM, Loqman MY, Miah G, Wahid H, et al (2013) A novel method for the synthesis of calcium carbonate (aragonite) nanoparticles from cockle shells. *Powder Technol* **235**, 70–5.
31. Kontoyannis CG, Vagenas NV (2000) Calcium carbonate phase analysis using XRD and FT-Raman spectroscopy. *Analyst* **125**, 251–5.
32. Bischoff JL (1969) Temperature controls on aragonite-calcite transformation in aqueous solution. *Am Mineral* **54**, 149–55.
33. Awang-Hazmi AJ, Zuki ABZ, Noordin MM, Jalila A, Norimah Y (2007) Mineral composition of the cockle (*Anadara granosa*) shells of west coast of Peninsular Malaysia and it's potential as biomaterial for use in bone repair. *J Anim Vet Adv* **6**, 591–4.
34. Bharatham BH, Zakaria MZAB, Perimal EK, Yusof LM, Hamid M (2014) Mineral and physiochemical evaluation of cockle shell (*Anadara granosa*) and other selected Molluscan shell as potential biomaterials. *Sains Malaysiana* **43**, 1023–9.
35. du Châtelet EA, Bout-Roumazeilles V, Coccioni R, Frontalini F, Guillot F, Kaminski MA, Recourt P, Riboulleau A, et al (2013) Environmental control on shell structure and composition of agglutinated foraminifera along a proximal-distal transect in the Marmara Sea. *Mar Geol* **335**, 114–28.
36. Annual Book of ASTM Standard (2014): F1185–03
37. Annual Book of ASTM Standard (2010): F1088–04a

RESEARCH ARTICLE
doi: 10.2306/scienceasia1513-1874.2018.44.397

ScienceAsia 44 (2018): **397–402**

Effect of curing temperature and time on the mechanical properties of hydroxyapatite/calcined kaolin

Ratchawoot Sutthi[a], **Nisanath Kaewwinud**[b], **Prinya Chindaprasirt**[c], **Yoshiharu Mutoh**[d], **Teerawat Laonapakul**[a,*]

[a] Department of Industrial Engineering, Faculty of Engineering, Khon Kaen University, Khon Kaen 40002 Thailand
[b] Engineering and Technology Management Program, Faculty of Industrial Technology, Surindra Rajabhat University, Surin 32000 Thailand
[c] Sustainable Infrastructure Research and Development Centre, Department of Civil Engineering, Faculty of Engineering, Khon Kaen University, Khon Kaen 40002 Thailand; and Academy of Science, The Royal Society of Thailand, Dusit, Bangkok 10300 Thailand
[d] (Professor Emeritus) Nagaoka University of Technology, Nagaoka, Niigata 940-2188 Japan

*Corresponding author, e-mail: teerla@kku.ac.th

Received 15 Jul 2018
Accepted 12 Dec 2018

ABSTRACT: In the current study, improvement of HAp/Calcined kaolin (CK) strength as a function of its curing regime was studied. The influence of curing temperature and time on the compressive strength of hydroxyapatite combined with calcined kaolin (HAp/CK) samples was investigated using statistical analysis. Curing temperatures were ranged 40, 60, 80 °C and curing times were 2, 7, 14, 21, 28 days, respectively. Prolonged curing time and increased curing temperature improved the compressive strength of the samples. The curing time and temperature significantly affected the compressive strength of HAp/CK samples, while there was no interaction between curing time and curing temperature. The highest compressive strength, 37.8 MPa, was realized by curing the sample at 80 °C for 28 days. The optimal process was curing HAp/CK at 60 °C for 14 days to achieve a high compressive strength.

KEYWORDS: compressive strength, bone substitute materials, calcium phosphate bioceramics, geopolymer

INTRODUCTION

Nowadays, a number of bone substitute materials including metals, polymers, and ceramics have been developed as alternatives for bone repair, augmentation or substitution[1]. The aim of development of bone substitutes is into create materials that have mechanical and chemical properties closest to those of human bone. Due to their bioactivity and biocompatibility, $Ca_3(PO_4)_2$ bioceramics, such as hydroxyapatite (HAp) and β-tricalcium phosphate (β-TCP), have been widely employed for bone repairs, fixing defects or filling voids. These are available in various forms, such as powders, porous scaffolds, blocks, or beads[2–4]. Unfortunately, low strength, fracture toughness and brittleness of HAp and β-TCP have limited its application to just bone repairs or low weight bearing monolithic implants. Geopolymer is a three-dimensional aluminosilicate polymeric structure, which consists of Si-O-Al bonds a chemical reaction between SiO_2 and Al_2O_3 under highly alkali conditions[5]. The materials that are currently attracting interest as bone substitutes or fillers are geopolymers and synthetic aluminosilicates[6–9]. Calcined kaolin (CK) is an aluminosilicate material that can be used as a starting material to obtain high strength geopolymers[10–13]. To produce biomaterials, clean source materials with minimum contamination are needed. The white coloured CK seems to be the best source material for this purpose.

On a review of literature, the property that is most often used to characterize the mechanical behaviour of bone substitute is their compressive strength. The compressive strength of porous human bone varies between 2 and 42 MPa for cancellous bone and between 100 and 230 MPa for cortical bone[14,15]. From previous research, mixtures of HAp with CK were investigated for their strengths and apatite formation[16]. The maximum compressive strength obtained from an HAp:CK mix at a ratio of

1:3 was 32.9 MPa when cured at 60 °C for 48 h. This HAp:CK material exhibited good bioactivity after immersion in simulated body fluids for 28 days. However, varying curing time and temperature may have substantial effects on the ultimate properties of the final product. This study investigated the improved strength of HAp mixed with CK in terms of the curing regime used. The effect of curing time and temperature on the compressive strength of the HAp:CK final product was also investigated. Statistical analysis was done to determine the level of influence of each factor. SPSS was used assuming a normal distribution. Two-way ANOVA and Duncan's multiple range tests were used in the statistical analysis.

MATERIALS AND METHODS

Preparation of starting materials

Hydroxyapatite (HAp) and calcined kaolin (CK) powders were used as the raw materials in this study. For the preparation of HAp powder, calcium carbonate ($CaCO_3$) produced from golden apple snail shell (calcined at 600 °C for 3 h[17]) and dicalcium phosphate dihydrate ($CaHPO_4 \cdot 2\,H_2O$, DCPD, Sigma Aldrich) were mechanochemically mixed at a theoretical stoichiometric Ca/P molar ratio (1.67) to produce HAp. This was done in a ball mill for 24 h. Then the material was heat-treated at a temperature of 1100 °C for 1 h. The crystalline phase of prepared HAp powder was identified using an X-ray diffraction equipment (XRD, Bruker D8). The XRD analysis was carried out with CuKα radiation operating at a scanning rate of 2.4 °C 2θ/min in 0.02 °C 2θ increment.

Calcined kaolin (CK) was prepared by calcination of metakaolin at a temperature of 600 °C in an electric furnace. The metakaolin used as the starting material was obtained from the eastern region of Thailand. Chemical composition of CK was determined using an X-ray fluorescence (WDXRF, AXios mAX). NaOH (10 M) and sodium silicate (15% Na_2O, 33% SiO_2 and 52% H_2O) with a mass ratio of 1.0 were used as a liquid activated binder for the HAp and CK powders.

Material preparation and evaluation

Hydroxyapatite (HAp) and calcined kaolin (CK) powders with an HAp:CK mass ratio of 1:3 (HAp/CK 25) was selected to study the influence of curing time and temperature on the compressive strength of the synthesized samples. This ratio was selected due to the high compressive strength and good bioactivity of samples prepared at this ratio[16]. The HAp/CK 25 powders were mechanically mixed with an activated binder solution using a planetary mixer for 5 min. The resulting sample paste was then rapidly poured into a $25\times25\times25$ mm^3 acyclic cube mould, and then mechanically vibrated for 10 s to remove entrapped air. Samples were carefully wrapped with a plastic film to prevent moisture loss. The cast samples were then separately cured in electric ovens.

In this study, two factors were varied, curing temperature and time, to investigate their effect on the compressive strength of HAp/CK 25. Three curing temperatures, 40, 60, and 80 °C, and five curing times, 2, 7, 14, 21, and 28 days, were evaluated. The samples cured for less than 28 days were removed from their moulds, wrapped in a plastic film and then stored at 23 °C until the 28 days. It has been reported that the temperature curing of 2 days produced geopolymer with a sufficiently high strength[18–20]. Hence the strength test at 2 days was performed in this experiment. Compressive strength tests were conducted on three cubed samples per each condition and the results were reported as the average values according to ASTM C109[21]. The statistical methods were employed to analyse the level of each factor using SPSS version 19.0. This analysis began with checking the adequacy of the model by testing the normality of the parameter value distributions for all treatments using Shapiro-Wilk's test (p-value > 0.05), since there were less than 50 data points. Then two-way ANOVA at a 95% confidence interval ($a = 0.05$) was employed to test the differences between the mean values. Duncan's multiple range test was used to compare the means of the five levels of curing times (2, 7, 14, 21, and 28 days) and the three levels of curing temperature (40, 60, and 80 °C).

RESULTS AND DISCUSSION

Characterization of starting materials

Fig. 1 shows the XRD pattern of the synthesized HAp powder. It was found from the figure that the major component of powder was HAp with a small amount of β-TCP in a crystalline phase. A similar behaviour was observed for HAp produced via a mechanochemical reaction[22–24]. Chemical composition of CK showed that it was composed mainly of 59% SiO_2, 36.71% Al_2O_3 1.43% TiO_2, 1% Fe_2O, 0.25% CaO 0.07% MgO and 0.03% SO_3.

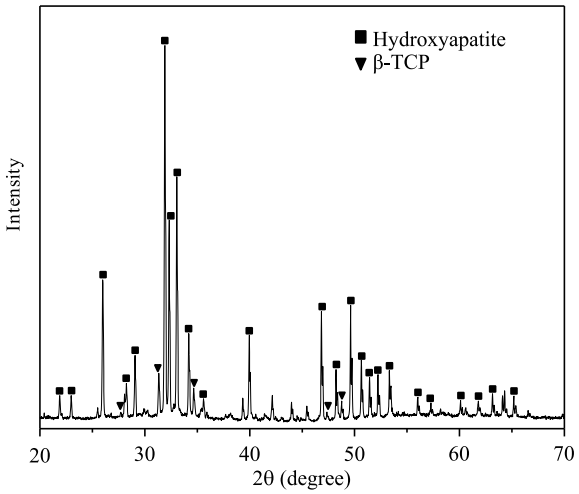

Fig. 1 XRD pattern of the hydroxyapatite synthesized from golden apple snail shell.

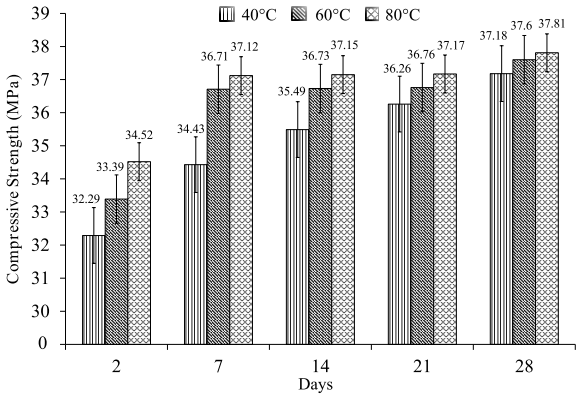

Fig. 2 Average compressive strengths of HAp/CK 25 samples after curing at 40, 60, and 80 °C for various curing periods

Compressive strength

The average compressive strengths of samples cured at 40, 60, and 80 °C with various curing times are shown in Fig. 2. These three different curing temperatures were selected from observations of kaolin-based geopolymers, indicating that heat is beneficial for strength development and curing at temperatures below 100 °C and that it has a significant contribution to the geopolymeric reaction in kaolin[25]. The curing times of 2, 7, 14, 21, and 28 days were selected to allow sufficient time for the geopolymerization process. From Fig. 2, it can be seen that the strength of the samples increased with increasing curing time at all temperatures. The strength linearly increased with increasing curing time for the samples cured at 40 °C whereas the strength of samples cured at 60 and 80 °C increased slightly over 7 days of curing. The highest strength, 37.8 MPa, was observed from samples cured at 80 °C for 28 days, while the compressive strength of cancellous bone is 2–45 MPa[14,15]. From these results, it can be concluded that the appropriate curing conditions are a temperature of 80 °C for at least 7 days for strong development of HAp/CK 25. This range of strength is potential for cancellous bone graft substitute. Statistical analyses were used to elucidate the influence of curing time and temperature on the strength of HAp/CK 25 samples.

Statistical analysis

The compressive strength of HAp/CK 25 was investigated using 15 treatments; five levels of curing time and three levels of curing temperature. Three replicates were made for each treatment and they were analysed statistically. The model adequacy was investigated using Shapiro-Wilk's test to verify data normality. The results show that the compressive strength data of HAp/CK 25 was normally distributed (p-value > 0.05) (Table 1). The results indicated that these data were adequate for further statistical analysis, assuming a normal distribution.

A two-way ANOVA at a 95% confidence interval was employed to investigate the effects of curing temperature and time on the compressive strength of HAp/CK 25. The factors were considered sep-

Table 1 Statistical data and Shapiro-Wilk's test of compressive strength of HAp:CK 25 using 15 treatments to test for normality.

	Day_Temp	Shapiro-Wilk		
		Statistic	df	Sig.
Strength	2_40	0.952	3	0.578
	2_60	1.000	3	1.000
	2_80	0.996	3	0.873
	7_40	0.980	3	0.729
	7_60	0.864	3	0.278
	7_80	0.864	3	0.278
	14_40	0.797	3	0.108
	14_60	0.999	3	0.935
	14_80	0.970	3	0.670
	21_40	0.945	3	0.549
	21_60	0.967	3	0.654
	21_80	0.827	3	0.181
	28_40	0.947	3	0.558
	28_60	0.999	3	0.956
	28_80	0.935	3	0.506

Table 2 Two-way ANOVA test of the effects of curing temperature and time on the compressive strength of HAp/CK 25. Tests factor: interaction effects; dependent variable: strength

Source	Type III SS	df	Mean Square	F	Sig.
C† Model	114.9[a]	14	8.2	6.3	0.0
Intercept	58 459.5	1	58 459.5	45 124.2	0.0
Day	88.6	4	22.2	17.1	0.0
temp	20.6	2	10.3	8.0	0.0
Day Temp	5.7	8	0.7	0.6	0.8
Error	38.9	30	1.3		
Total	58 613.3	45			
C† Total	153.8	44			

[a] $R^2 = 0.747$ (Adjusted $R^2 = 0.629$). Type III SS = Type III sum of squares. C† = corrected.

Table 3 Pearson correlation of curing time and curing temperature with the compressive strength of HAp/CK 25.

		Day	Temp	Strength
Day	Pearson correlation	1	0.000	0.660
	Sig. (2-tailed)		1.000	0.000
	N	45	45	45
Temp	Pearson correlation	0.000	1	0.359
	Sig. (2-tailed)	1.000		0.016
	N	45	45	45
Strength	Pearson correlation	0.660	0.359	1
	Sig. (2-tailed)	0.000	0.016	
	N	45	45	45

Table 4 Duncan's multiple range test of curing temperature and curing time on the compressive strength of HAp/CK 25.

C† time	N	Subset			C† temp.	N	Subset	
		1	2	3			1	2
2.00	9	33.4			40.0	15	35.1	
7.00	9		36.1		60.0	15		36.2
14.0	9		36.5	36.5	80.0	15		36.8
21.0	9		36.7	36.7	Sig.		1.0	0.2
28.0	9			37.5				
Sig.		1.0	0.3	0.1				

N = Sample size, Sig. = Significance. C† = cured.

arately and in aggregate. The results are shown in Table 2. The ANOVA results revealed that both curing time and curing temperature significantly affected (p-value < 0.05) the compressive strength of HAp/CK 25, while the interaction between curing time and curing temperature showed no significant effect (p-value > 0.05) on the compressive strength of HAp/CK 25, (Table 2).

Furthermore, the Pearson correlation coefficient (Table 3) showed that the effects of curing time and temperature on compressive strength are related in a positive linear sense. The correlation value between curing time and compressive strength was 0.660 and between curing temperature and compressive strength was 0.359. This means the compressive strength of HAp/CK 25 increased with increasing curing time. Also, at a higher curing temperature, the compressive strength was greater than at a lower curing temperature. Furthermore, it was found that the correlation between curing time and compressive strength was much stronger than that between curing temperature and compressive strength ($0.660 > 0.359$) as shown in Table 3. Many studies on geopolymers conformed that curing temperature and curing time significantly influence the compressive strength [19, 20, 26, 27].

Duncan's multiple range test was then used to compare the range of a subset of the compressive strengths of HAp/CK 25 based on curing time and another range of a subset of the compressive strengths of HAp/CK 25 based on curing temperature. The results are shown in Table 4.

The compressive strength of HAp/CK 25 increased significantly with increased curing time. However, there were no significant differences in the compressive strengths of HAp/CK 25 after 7, 14, and 21 days of curing at a 95% confidence interval. The highest compressive strength, 36.7 MPa, was observed after 21 days. Furthermore, after 14, 21, and 28 days of curing, there were no significant differences in the compressive strengths of HAp/CK 25 at a 95% confidence interval. The highest compressive strength, 37.5 MPa, was after 28 days.

The compressive strength of HAp/CK 25 increased significantly with increased curing temperature. There were significant differences in compressive strength of HAp/CK 25 with curing at 40 °C among all pairs of curing temperatures at a 95% confidence interval. However, there were no significant differences in compressive strength of HAp/CK 25 with curing at 60 °C and 80 °C with a 95% confidence interval. The highest compressive strength, 36.8 MPa, was observed after curing at 80 °C. From these results, it can be concluded that curing at 60 °C for 14 days represents the optimal curing conditions to achieve the maximal compressive strength of HAp/CK 25. Future research is required to evaluate the bioactivity and other mechanical and physical properties, such as bending

strength, porosity, surface morphology of HAp/CK 25 under optimal curing condition.

CONCLUSIONS

The effects of curing time (2, 7, 14, 21, and 28 days) and temperature (40 °C, 60 °C and 80 °C) of hydroxyapatite combined with calcined kaolin (1:3 mass ratio) were investigated. Statistical analyses were used to determine the level of influence of each factor. The conclusions of the current study are as follows.

(1) The compressive strength of the HAp/CK 25 increased significantly with increasing curing temperature and curing time.
(2) The highest compressive strength of HAp/CK 25, 37.8 MPa, was achieved after curing the sample at 80 °C for 28 days.
(3) Statistical analyses revealed that both curing temperature and curing time significantly affected compressive strength, while there were no interactions between these two factors.
(4) The optimal curing conditions for HAp/CK 25 to achieve its highest compressive strength was 60 °C for 14 days.
(5) The combinations between HAp/CK 25 provided suitably high compressive strength for the bone substitute material.

Acknowledgements: This study was supported by the Capacity Building Program for New Researcher 2018 from National Research Council of Thailand (NRCT). The third author would like to acknowledge the support of Thailand Research Fund (TRF) under the TRF Distinguished Research Professor Grant No. DPG6180002. The last author would like to acknowledge the support of the Thailand Research Fund and the Office of the Higher Education Commission Grant No. MRG6180026 and the Farm Engineering and Automatic Control Technology Research Group (FEAT), Khon Kaen University, Thailand.

REFERENCES

1. Wang W, Yeung K WK (2017) Bone grafts and biomaterials substitutes for bone defect repair: A review. *Bioact Mater* **4**, 224–47.
2. Benmarouane A, Hansen T, Lodini A (2004) Heat treatment of bovine bone preceding spatially resolved texture investigation by neutron diffraction. *Physica B* **350**, 1–3.
3. Arahira T, Maruta M, Matsuya S, Todo M (2015) Development and characterization of a novel porous β-TCP scaffold with a three-dimensional PLLA network structure for use in bone tissue engineering. *Mater Lett* **152**, 148–50.
4. Chen Q, Roether JA, Boccaccini AR (2008) Tissue engineering scaffolds from bioactive glass and composite materials. *Tissue Eng* **4**, 1–27.
5. Hassaan MM, Khater HM, El-Mahllawy M S, El Nagar AM (2015) Production of geopolymer composites enhanced by nano-kaolin material. *J Adv Ceram* **4**, 245–52.
6. Catauro M, Bollino F, Papale F, Lamanna G (2014) Investigation of the sample preparation and curing treatment effects on mechanical properties and bioactivity of silica rich metakaolin geopolymer. *Mater Sci Eng: C* **36**, 20–4.
7. Pangdaeng S, Sata V, Aguiar J B, Pacheco-Torgal F, Chindaprasirt P (2015) Apatite formation on calcined kaolin-white Portland cement geopolymer. *Mater Sci Eng: C* **51**, 1–6.
8. MacKenzie KJ, Rahner N (2010) Calcium-containing inorganic polymers as potential bioactive materials. *J Mater Sci* **45**, 999–1007.
9. Oudadesse H, Derrien AC, Martin S, Chaair H, Cathelineau G (2008) Surface and interface investigation of aluminosilicate biomaterial by the 'in vivo' experiments. *Appl Surf Sci* **255**, 593–6.
10. Davidovits J (1999) Chemistry of Geopolymeric Systems. Terminology In Proceedings of 99 International Conference, France, pp 9.
11. Van Jaarsveld JG, Van Deventer JS, Lukey GC (2003) The characterization of source materials in fly ash-based geopolymers. *Mater Lett* **57**, 1272–80.
12. Swanepoel JC, Strydom CA (2002) Utilization of fly ash in a geopolymeric material. *Appl Geochem* **17**, 1143–8.
13. RovnanÃ◌k P (2010) Effect of curing temperature on the development of hard structure of metakaolin-based geopolymer. *Constr Build Mater* **24**, 1176–83.
14. Hannink G, Arts JC (2011) Bioresorbability, porosity and mechanical strength of bone substitutes: what is optimal for bone regeneration? *Injury* **42**, 22–5.
15. Sopyan I, Mel M, Ramesh S, Khalid KA (2007) Porous hydroxyapatite for artificial bone applications. *Sci Technol Adv Mater* **8**, 116–23.
16. Sutthi R, Pangdaeng S, Chindaprasirt P, Otsuka Y, Mutoh Y, Laonapakul T (2017) Hydroxyapatite from golden apple snail shell with calcined kaolin for biomaterial applications. *Key Eng Mater* **718**, 133–8.
17. Leelatawonchai P, Laonapakul T (2014) Preparation and characterization of calcium sources from golden apple snail shell for naturally based biomaterials. *Adv Mater Res* **931**, 370–4.
18. Chindaprasirt P, Jaturapitakkul C, Chalee W, Rattanasak U (2009) Comparative study on the characteristics of fly ash and bottom ash geopolymers. *Waste Manage* **29**, 539–43.
19. Khale D, Chaudhary R (2007) Mechanism of geopolymerization and factors influencing its development: a review. *J Mater Sci* **42**, 729–46.
20. Mo BH, Zhu H, Cui XM, He Y, Gong SY (2014)

Effect of curing temperature on geopolymerization of metakaolin-based geopolymers. *Appl Clay Sci* **99**, 144–8.
21. ASTM C109 (2005) Standard test method of compressive strength of hydraulic cement mortars (using 2-in. [or 50 mm] cube specimens) *Annual Book of ASTM Standard* pp 76–81.
22. Suchanek WL, Shuk P, Byrappa K, Riman RE, TenHuisen KS, Janas VF (2002) Mechanochemical-hydrothermal synthesis of carbonated apatite powders at room temperature. *Biomaterials* **23**, 699–710.
23. Yeong K CB, Wang J, Ng SS (2001) Mechanochemical synthesis of nanocrystalline hydroxyapatite from CaO and $CaHPO_4$. *Biomaterials* **22**, 2705–12.
24. Rhee SH (2002) Synthesis of hydroxyapatite via mechanochemical treatment. *Biomaterials* **23**, 1147–52.
25. Heah CY, Kamarudin H, Al Bakri AM, Binhussain M, Luqman M, Nizar I K, et al (2011) Effect of Curing Profile on Kaolin-based Geopolymers. *Physics Procedia* **22**, 305–11.
26. Mishra A, Choudhary D, Jain N, Kumar M, Sharda N, Dutt D (2008) Effect of concentration of alkaline liquid and curing time on strength and water absorption of geopolymer concrete. *ARPN Journal of engineering and Applied Sciences* **3**, 14–8.
27. Torkittikul P, Chaipanich A (2009) Investigation of the mechanical and in vitro biological properties of ordinary and white Portland cements. *ScienceAsia* **35**, 358–64.